NASS
NAN YANG ACADEMY OF SCIENCES

Earth and Planetary Science

Volume 1 · Issue 2 · October 2022 ISSN 2810-9732

Volume 1 Issue 2 • October 2022 ISSN 2810-9732 (Online)

Earth and Planetary Science

NASS
NAN YANG ACADEMY OF SCIENCES

NASS
NAN YANG ACADEMY OF SCIENCES

Volume 1 | Issue 2 | October 2022 | Page1-34
Earth and Planetary Science

Contents

Research Articles

Review Article

Earth and Planetary Science
https://ojs.nassg.org/index.php/eps/index

RESEARCH ARTICLE

Petrological and Geochemical Characteristics of Al-rich Pelitic Granulites/Paragneiss from Thana, District-Bhilwara Rajasthan: Implication for Its Origin

Harel Thomas* **Jyoti Bidolya** **Aman Soni** **Rishabh Batri**

Department of Applied Geology, Dr. Harisingh Gour Vishwavidyalaya (A Central University), Sagar (M.P.), 470003, India

ARTICLE INFO

Article history
Received: 23 June 2022
Revised: 25 July 2022
Accepted: 29 July 2022
Published Online: 10 August 2022

Keywords:
Petrogeochemistry
Protolith
Al-rich pelitic granulites/paragneiss
Tectonic settings and origin

ABSTRACT

Al-rich pelitic granulites/paragneiss are frequently observed in the medium- to high-grade metamorphic rocks of Thana. It is dominantly composed of sillimanite-kyanite-garnet-biotite-plagioclase-k-feldspar and a subordinate amount of quartz. Garnet both xenoblastic as well as idioblastic is wrapped around by flaky minerals. These Al-rich pelitic granulites are the result of the metamorphism of pre-existing sedimentary rocks under medium to high grade P-T conditions and consist essentially of sillimanite-kyanite-staurolite-garnet-biotite bearing Al-rich pelitic granulites/paragneiss. The geochemical data reflect that Thana pelitic granulite is of S-type and peraluminous in nature. Geochemically, the protolith for these Al-rich pelitic granulites/paragneiss is shale or greywacke. Paper records the petrography, geochemical characters and probable origin of these Al-rich pelitic granulites/paragneiss.

1. Introduction

The granulites of Rajasthan occur as enclaves in the Banded Gneissic Complex (BGC), Heron (1917, 1935 and 1953) [1-3] and Gupta (1934) [4]. It is dominantly composed of sillimanite-kyanite-garnet-biotite-plagioclase-k-feldspar and a subordinate amount of quartz. Garnet both xenoblastic as well as idioblastic is wrapped round by flaky minerals. Geochronological studies indicate that the granulites evolved during the late-Paleoproterozoic between ca. 1725 and ca. 1622 Ma Sarkar et al. (1989) [5]; Joshi et al., (1993) [6]; Fareeduddin et al., (1994) [7] and Roy et al., (2005) [8]; Buick et al., (2006) [9]; Rao et al., (2011) [10] The granulite facies rocks include charnockite/enderbite, mafic granulites, khondalites, leptynites and Al-Mg riched metapelites, reported by Sharma, R.S., (1977, 1988 and 1999) [11-13]; Joshi et al., (1993) [14] and Thomas (1995 and 2005) [15,16]; Thomas and Sujata (2008) [17], Thomas and Neeraj, (2011a and b) [18,19]; Thomas and Lalu, (2014) [20]; Kavita and Thomas, (2018) [21], Neeraj and Thomas, (2015) [22] and Thomas, H., and Rana, H. (2020) [23]. Al-rich pelitic granulites/paragneiss are the special type of mixed meta-

*Corresponding Author:
Harel Thomas,
Department of Applied Geology, Dr. Harisingh Gour Vishwavidyalaya (A Central University), Sagar (M.P.), 470003, India;
Email: hthomas@dhsgsu.edu.in

DOI: https://doi.org/10.30564/eps.v1i2.564

morphic of Bhilwara Complex Gupta (1934) [4]. These rocks developed in the SW of Thana area (Figure 1). They are predominantly kyanite-sillimanite-garnet-biotite gneiss. Between Thana and Shivpura village the paragneiss is embedded in hornblende-biotite gneiss. In the NE of Thana and near Shivpura the paragneiss banding becomes thin and small and the rocks contain sillimanite-garnet and staurolite-kyanite-garnet. Small lensoid bodies containing enderbite and metanorite were found in paragneiss in NE of Thana and Shivpura villages. The main rock types exposed in the area are pelitic granulite/paragneiss, charnockite/enderbite, metanorite, gneisses. The main aim of the present paper is to: (i) provide petrographic and geochemical characteristics of pelitic granulite/paragneiss; (ii) find out the petrogenesis of pelitic granulite/paragneiss; (iii) placement of these rocks in the tectonic history of the banded gneissic complex of central Rajasthan.

2. Geological Setting

Heron (1917, 1935 and 1953) [1-3] and Gupta (1934, Figure 1) [4] have classified the Precambrian metamorphic rocks of Rajasthan into four stratigraphic units. They introduced the term "Banded Gneissic Complex" to designate the Archaean Basement rocks of the Central Mewar region. The different geological formations of Central Mewar (which includes the present Udaipur and Bhilwara districts) are summarized after Gupta (1934) [4] in Tables 1 and 2.

The Sand Mata rocks mapped by Gupta (1934) [4] have been designated by him as Sand Mata paragneiss complex of Pre-Aravalli age. However, in the accompanying map of his Memoir, these paragneisses have been erroneously shown under the Aravalli System, the rocks which unconformably overlie the BGC rocks in Rajasthan. Gupta (1934, Figure 1) [4] called these rocks as "special type of mixed rocks of metamorphic origin" and recognized them as undoubtedly meta-sedimentary rocks of the Pre-Aravalli age. Gupta et al., (1980 and 1997) [24,25] divided the BGC of Central Rajasthan into two tectonic-cum-metamorphic domains i.e. the Sand Mata Complex (granulite facies rocks) towards west and the Mangalwara Complex (amphibolite facies rocks) towards east, which are separated by the northsouth Delwara lineament. In the investigated area, only the Banded Gneissic Complex of Bhilwara Supergroup is exposed and the detailed sequence of the Pre-Aravalli (after Gupta, 1934, p. III) [4], from oldest to youngest is as follows (Table 2):

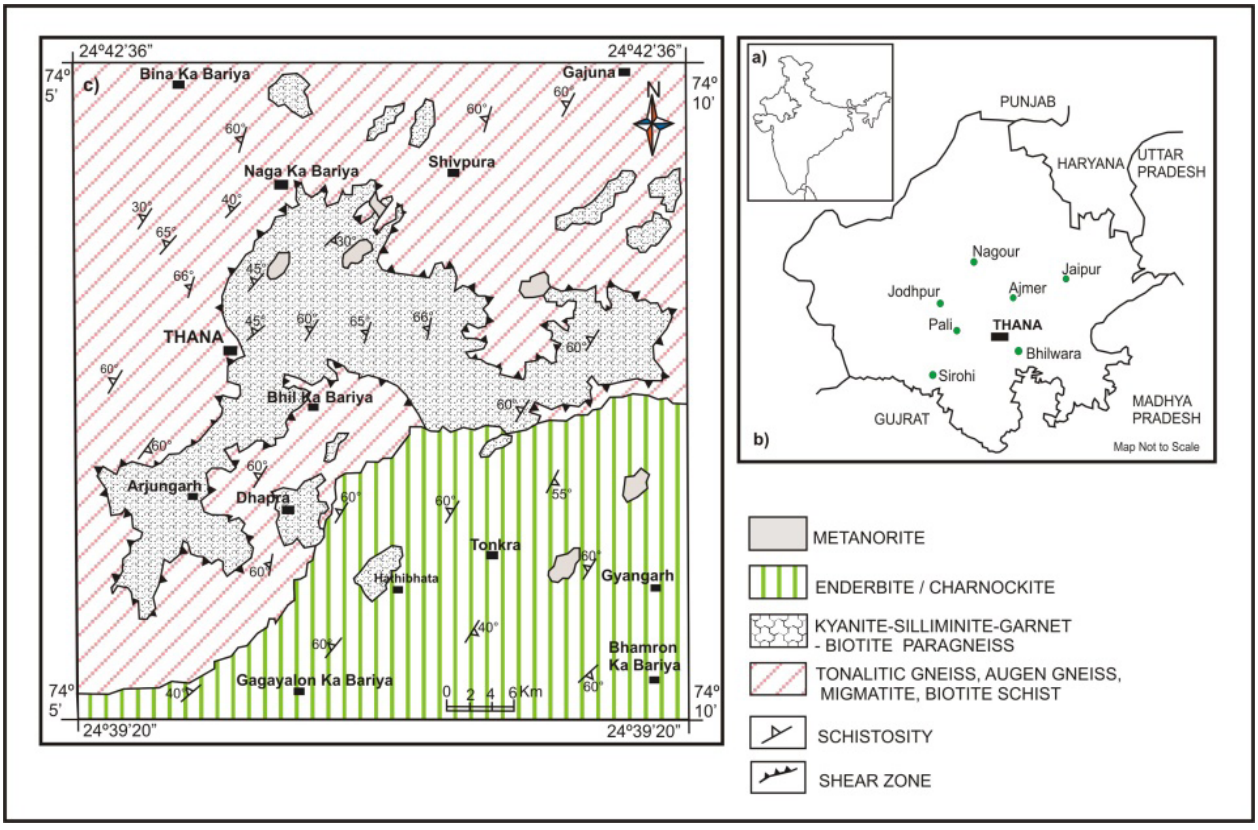

Figure 1. Geological map around Thana, Bhilwara, Rajasthan by author [1], showing different lithounits.

Table 1. The different geological formations of Central Mewar (which includes present Udaipur and Bhilwara districts) are summarized after Gupta (1934) [4] and Gupta et al., 1997 [25].

Mesozoic & Cenozoic		**Deccan Traps, Tertiary Alkaline Complex, Sedimentary and Quaternary sediments**
Palaeozoic		
Proterozoic	Marwar Supergroup	Jodhpur Group, Bilara Group, Nagaur Group
	Malani Igneous Supergroup	
	Vindhyan Supergroup	Lower Vindhyan Group, Upper Vindhyan Group
	Delhi Supergroup	Railo Group, Alwar Group, Ajabgarh Group, Gogunda Group, Khumbhalgarh Group, Sirohi, Punagarh Group, Sindreth Group
	Aravalli Supergroup	Debari Group,Udaipur Group, Bari Lake Group, Kankroli Groupv, Jharol Group, Dovda Group, Nathdwara Group, Lunavada Group
	Bhilwara Supergroup	Rajpur-Dariba Group, Pur-Banera Group, Jahazpur Group, Sawar Group, Ranthambor Group
Archaean	Bhilwara Supergroup	Sandmata Complex, Mangalwara Complex, Hindoli Group

Table 2. The different geological formations of Central Mewar (which includes present Udaipur and Bhilwara districts) are summarized after Gupta (1934) [4].

	------ Paragneiss (Sand Mata)
	------ Dolerite
Banded Gneissic	------ Schist
Complex	------ Quartz Veins
(Bhilwara Supergroup)	------- Pegmatite
	------- Granite
	------- Aplite
	--------Amphibolite (Epidiorite)

3. Petrography

Al-rich pelitic granulites/paragneiss occupy a substantial portion of the explored area. They are dark, greenish to light in colour and contain garnet, sillimanite, kyanite, staurolite, biotite, K-feldspar, plagioclase, quartz and secondary muscovite and chlorite in several assortments. On the basis of paragenesis, the Al-rich pelitic rocks can be categorized into five major groups.

i. Kyanite-staurolite-garnet-bearing paragneiss
ii. Kyanite-biotite-garnet bearing paragneiss
iii. Sillimanite-garnet-biotite bearing paragneiss
iv. Sillimanite-Kyanite-garnet-biotite bearing paragneiss
v. Andalusite-kyanite-sillimanite-garnet-bearing gneiss

Regardless of the variation in mineralogy and texture, their petrography has been described concurrently to avoid repetition.

Kyanite-Staurolite-Garnet bearing gneiss megascopic characters

The rocks are dark greenish to light, fine to coarse grained with well-developed foliations. Two sets of foliations are evident by the orientation of kyanite, sillimanite, biotite and secondary muscovite.

Microstructure/Texture

The texture is granoblastic to schistose. Garnet and andalusite occur as porphyroblasts, in a few sections, reaction rims of garnet are present around biotite and kyanite/sillimanite and hornfelsic texture is also observed.

Kyanite-Staurolite-Garnet-bearing paragneiss

Kyanite-staurolite-garnet-quartz with secondary muscovite (Sample No.R87/438).

Kyanite-Biotite-Garnet bearing paragneiss

Kyanite-garnet-biotite-kyanite needles-quartz-k-feldspar-plagioclase-sericite-magnetite (Sample No. R87/347).

Sillimanite-Garnet-Biotite bearing paragneiss

Sillimanite-biotite-garnet-quartz-k-feldspar-plagioclase (secondary muscovite-chlorite)-rutile (Sample No. R87/407).

Kyanite-Sillimanite-Biotite-Garnet bearing paragneiss

Sillimanite-kyanite-garnet-biotite-quartz-(secondary muscovite)-K-feldspar-plagioclase-ilmenite (Sample No. R87/248 & 250).

Andalusite-Kyanite-Sillimanite-Garnet bearing gneiss

Andalusite-garnet-biotite-quartz-epidote-magnetite-k-feldspar (Sample No. R87/452).

Microscopic description of minerals

Kyanite

Prisms of varying sizes are interleaved with biotite showing a significant dimensional orientation in a few

sections kyanite appears to wrap around garnet porphyroblasts. Its association with garnet, biotite and staurolite suggests the following reactions:

Staurolite + quartz = kyanite + garnet

Biotite + kyanite + quartz = garnet + k-feldspar

The first generation kyanite has broad blades which are scarcely folded. The later generation kyanite is characterized by acicular form and random orientation; they may be called needle kyanite.

Sillimanite

Sillimanite occurs as rectangular to short crystals it envelopes small blades of kyanite and shows cross-cutting relationship with early generation kyanite (KY1). In a few sections sillimanite shows microscopic folding and sometimes sillimanite merges into kyanite needles, these features reveal that the sillimanite event occurred between kyanite (1) and needle kyanite (2).

Garnet

Garnet sizes ranging from 0.4 mm to 0.6 mm few grains are elongated along the fracture plane and have an inclusion of kyanite, biotite, quartz, magnetite, staurolite, rutile and sphene. Garnet is marginally altered into chlorite and, suggests the reaction

Garnet+ fluid = chlorite + quartz + magnetite

Staurolite

Crystals are short prismatic and show a prominent dimensional orientation; it shows sharp contact with garnet and kyanite and appears as inclusions in garnet, indicating the following reactions:

Staurolite + Quartz = Garnet + Kyanite

Biotite

Garnet laths are reddish brown; pleochroism varies from red brown to light brown. Pleochroic haloes around zircon grains are common and biotite shows a clear textural relation with kyanite and sillimanite and imparts an appreciable foliation to the rock. The corroded outline of the biotite and its textural relation with fresh garnet and k-feldspar indicate the following reaction.

Biotite + Sillimanite + Quartz = Garnet + K-feldspar + Water

K-feldspar

It is mostly microcline with clear cross-hatched twinning. Microcline porphyroblasts have inclusions of biotite, kyanite/sillimanite and, garnet which suggests the reaction:

Garnet + K-feldspar + Water = Biotite + Kyanite/Sillimanite + Quartz

Plagioclase

Plagioclase is invariably present in the rocks. The grains are twinned on the albite and Carlsbad laws.

Quartz

Quartz is mainly xenoblastic in shape showing wavy extinction. Quartz is also found as an inclusion in garnet and shows sharp contact with all minerals except staurolite.

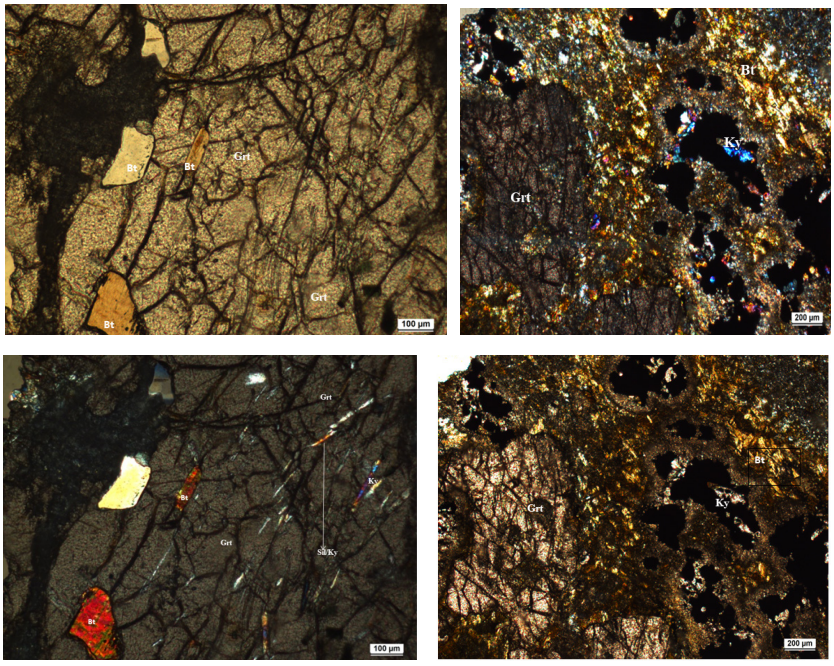

Photomicrography: (A & B) garnet porphyroblast showing irregular fractures along with inclusions of biotite and kyanite/sillimanite (sample No. R87/423); Photomicrograph (C & D) showing kyanite interleaved with biotite.

4. Geochemistry and Petrogenesis of Al-rich Pelitic Granulites/Paragneiss

Results of the fifteen selected rock samples of paragneiss/Al-rich pelitic assemblages were analyzed by Atomic absorption spectrometry (AAS) and flame photometry from the Wadia Institute of Himalayan Geology. The major elements, trace elements in (ppm) and Niggli values are shown in Tables 3, 4 and 5 respectively. The rocks of different assemblages show clear chemical differences. The calculated Niggli values are shown in Table 3.

The SiO_2 and Al_2O_3 contents fluctuate between 45.2% to 68.28% wt% and 13.10% to 25.2% wt% respectively. In all the fifteen samples the SiO_2 content is generally > 45% whereas the percentage of Al_2O_3 content is higher in R87/397, R87/293 and R87/342. The ACF and AKF diagrams (Figure 2) clearly indicate that all samples lie within the pelitic field. The rocks have an average Na_2O and K_2O concentration of 1.30% and 2.99% respectively and the average K_2O/Na_2O ratio is 2.3 and their TiO_2 content varies from 0.48% to 2.08%.

Table 3. Major element analyses (wt%) of the Al-rich pelitic granulites/paragneiss from the Thana and adjoining area, district Bhilwara, Rajasthan.

S. No.	Sample NO.	SiO_2	Al_2O_3	Fe_2O_3	FeO	MgO	CaO	Na_2O	K_2O	MnO	TiO_2	P_2O_5	Total
1	R87/291	50.75	22.26	2.6	10.48	4.64	2.8	0.8	2.4	0.103	0.99	0.16	97.983
2	R87/293	45.2	25.27	2.4	12	4.64	2.2	1	3.4	0.065	1.4	0.09	98.065
3	R87/299	58.13	18.07	2.47	9.92	3.63	2.8	0.8	2.1	0.131	0.723		98.774
4	R87/342	49.8	24.35	3.6	11.17	3.43	2.24	1	1.2	0.17	0.84	0.2	98
5	R87/ 368	68.28	13.1	1.42	4.34	1.41	3.36	3.04	3.1	0.048	1.015	0.27	99.743
6	R87/377	58.13	21.20	1.76	6.56	2.42	2.8	1	3.8	0.037	0.907	0.15	98.764
7	R87/392	69.2	13.9	2.48	5.59	2.02	2.8	1.2	1.7	0.04	0.853	0.13	99.913
8	R87/397	49.8	25.14	3.12	9.08	2.22	3.36	1.2	3.4	0.054	1.123	0.12	98.617
9	R87/409	65.51	14.7	1.37	6.2	1.61	5.6	2	1.4	0.076	0.713	-	99.179
10	R87/423	60.9	20.2	1.9	5.85	2.62	2.25	1.4	3.1	0.06	0.756	-	99.036
11	R87/442	57.21	20.95	1.72	7.17	2.82	3.08	1	3.6	0.078	0.89	0.095	98.613
12	R87/477	65.51	19.38	1.07	4.12	0.6	3.36	1	3.7	0.046	0.48	-	99.246
13	R87/478	58.13	17.55	2.2	12.8	3.02	2.8	0.8	2.2	0.07	1.14	0.13	100.84
14	91/518	66.08	21.28	-	4.99	3.18	0.1	0.29	3.25	-	0.83	-	100
15	91/544	52.31	21.45	-	6.45	4.78	3.03	3.06	6.61	0.14	2.08	-	99.98

Table 4. Trace element (in ppm) of the Al-rich pelitic granulites/paragneiss from the Thana and adjoining area, district Bhilwara, Rajasthan.

Ref. No.	Sample No.	Cu	Co	Li	Ni	Rb	Sr	V	Zn	Rb / Sr
1	R87/291	165	11	22	33	96	68	92	188	1.41
2	R87/293	75	14	26	39	126	31	225	240	4.06
3	R87/299	165	9	8	26	81	76	92	148	1.06
4	R87/342	86	13	9	38	68	47	200	186	1.45
5	R87/ 368	174	9	11	26	103	188	108	147	0.55
6	R87/377	156	9	38	28	183	65	120	140	2.81
7	R87/392	189	9	12	25	68	52	135	161	1.31
8	R87/397	176	12	13	32	73	298	216	204	0.24
9	R87/409	222	9	15	27	53	199	108	107	0.27
10	R87/423	290	10	4	29	161	140	90	156	1.15
11	R87/442	200	13	19	31	93	95	240	126	0.97
12	R87/477	262	7	15	20	89	129	120	136	0.69
13	R87/478	224	11	17	36	91	26	160	234	3.50
Average		183.38	10.61	15.15	30	98.84	108.77	146.62	167.15	0.91

Table 5. Niggli values of Al-rich pelitic granulites/paragneiss from Thana, Bhilwara, Rajasthan.

Sample no.	al	alk	C	mg	fm	Si	ti	p	k
R87/291	36.3	6.37	8.3	0.39	49	140.5	2.04	0.18	0.6
R87/293	38.36	6.95	5.97	0.367	47.7	114.66	2.66	0.09	0.69
R87/299	33.8	6.7	9.5	0.34	49.86	184.8	1.7	-	0.6
R87/342	40.1	4.83	6.7	0.295	48.3	139.2	1.7	0.23	0.44
R87/368	32.96	22.49	15.36	0.36	29.16	291.6	3.25	0.48	0.37
R87/377	42.5	11.56	10.22	0.345	35.6	198.2	2.32	0.21	0.71
R87/392	35.58	9.75	13.2	0.314	41.63	300.68	2.78	0.273	0.48
R87/397	42.28	9.5	10.27	0.25	37.93	142.16	2.4	0.149	0.65
R87/399	33.0	11	23	0.28	33	250	2	-	0.315
R87/423	42.64	11.92	8.63	0.37	36.79	218.26	2.02	-	0.59
R87/442	40.5	10.7	10.8	0.36	37.9	187.9	2.1	0.11	0.7
R87/477	48.53	14.14	15.29	0.172	22.02	278.47	1.46	-	0.788
R87/478	31.88	6.71	9.24	0.265	52.15	179.25	2.64	0.16	0.644
R87/518	52.36	9.85	0.45	0.534	37.34	276.38	2.59	-	0.881
R87/544	35.34	20.11	9.09	0.566	35.46	146.49	4.37	-	0.588

The Harker variation diagrams between SiO_2 and others major oxides (FeO, MgO, Al_2O_3, TiO_2, MnO, Fe_2O_3, K_2O, Na_2O, CaO and P_2O_5; Figure 3a to 3j) shows good correlations which indicates coherent behaviours of element during different processes of metamorphism.

The trace elemental geochemistry of Al-rich pelitic granulites/paragneiss show variable concentration of Cu (75 ppm to 290 ppm; average 83.38 ppm); Li (4 ppm to 38 ppm; average 15.15 ppm); Ni (20 ppm to 39 ppm; average 30 ppm.); Co (7 ppm to 14 ppm; average 10.61 ppm); V (90 ppm to 240 ppm; average 146.62); Zn (107 ppm to 240 ppm; average 167.15 ppm.); Rb (53 ppm to 183 ppm; average 98.84 ppm) and Sr (26 ppm to 298 ppm; average 108.77 ppm) and are enriched in comparison to Rb.

The Harker diagrams between SiO_2 and trace elements (Cu, Li, Ni, Rb, Sr, Co, Zn and V; Figures 4a to 4f), show good correlations, while Rb and Sr show poor correlations, which means the system is more evolved. The Rb/Sr ratios range in between 0.24 ppm to 4.06 ppm and average 0.91 ppm suggestion depletion of Sr.

The Niggli values in Table 3, indicate the silica saturated nature of the Al-rich pelitic granulites/paragneiss. The Niggli values show that the rocks are higher in Al/Alk ratio with an average of 3.60 and low mg number which suggest a highly evolved system.

The plot between K_2O/Al_2O_3 and Na_2O/Al_2O_3 (Figure 5) has clearly differentiated the sedimentary from igneous rocks, Garrels and Machenzie (1971) [26]. It is evident that all samples fall within the field specified for sedimentary rock.

The plots between Al_2O_3 against ($K_2O + Na_2O$) (Figure 6) after Goel, and Chaudhari, (1979) [27] also indicate all samples fall within the sedimentary bearing field. Similarly A-CN-K diagram (Figure 7) after Nesbitt, et al., (2003) [28] also shows sedimentary fields. The chemical variations have also been studied with the help of Niggli values. The 'mg' versus 'c' diagram (Figure 8) most of the samples lie in the pelitic and semi-pelite field Leake, (1964) [29]. Only two samples lie outside this field, this could be due to the post metamorphic changes during poly-metamorphism.

The diagram SiO_2/Al_2O_3 versus K_2O/Na_2O (Figure 9) shows A, B, C and D the compositional fields of pelitic greywacke, pelites, greywacke and arkose Wimmenaure and Fortscher (1984) [30] and the compositional field of greywacke and shale, Condie, et al., (1991) [31], respectively. It is evident from the diagram that most samples fall within the pelitic field specified by Condie, et al., (1991) [31] However, some samples are scattered due to the poly metamorphism or partially metasomatism.

The Niggli values are also used to examine the nature of the protolith. When the values are plotted in the 100 mg-c-(al-alk) diagram (Figure 10) Leake, (1964) [29] all the samples fall within the shale-field Leake, (1964) [29], when c values are plotted against (al-alk) (Figure 11) [26] of the samples fall within the shale and greywacke filed. Few samples show slight scattering which may be due to the poly-metamorphism.

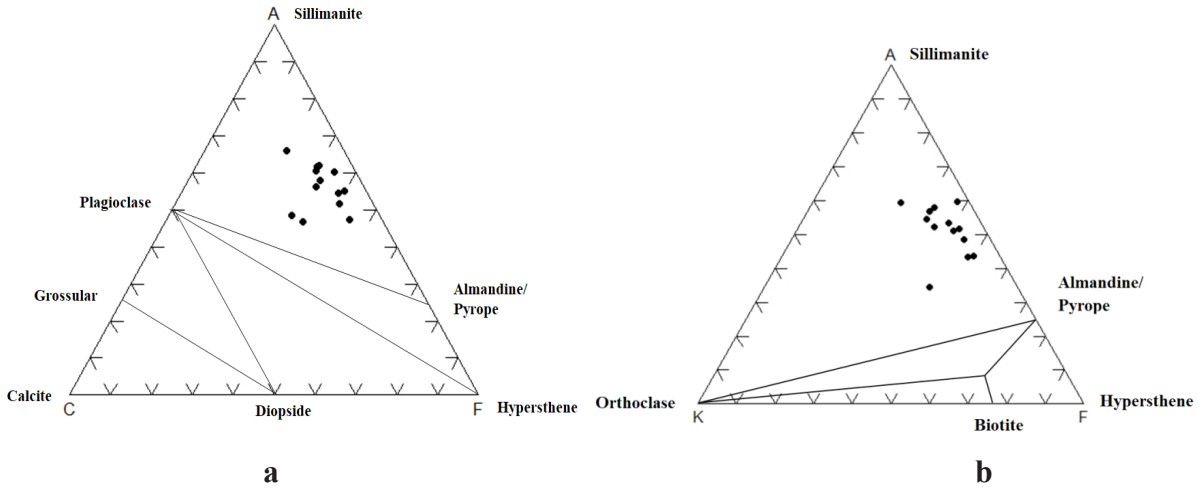

Figure 2. ACF and AKF diagrams showing chemical analysis of Al-rich pelitic granulites/paragneiss from Thana.

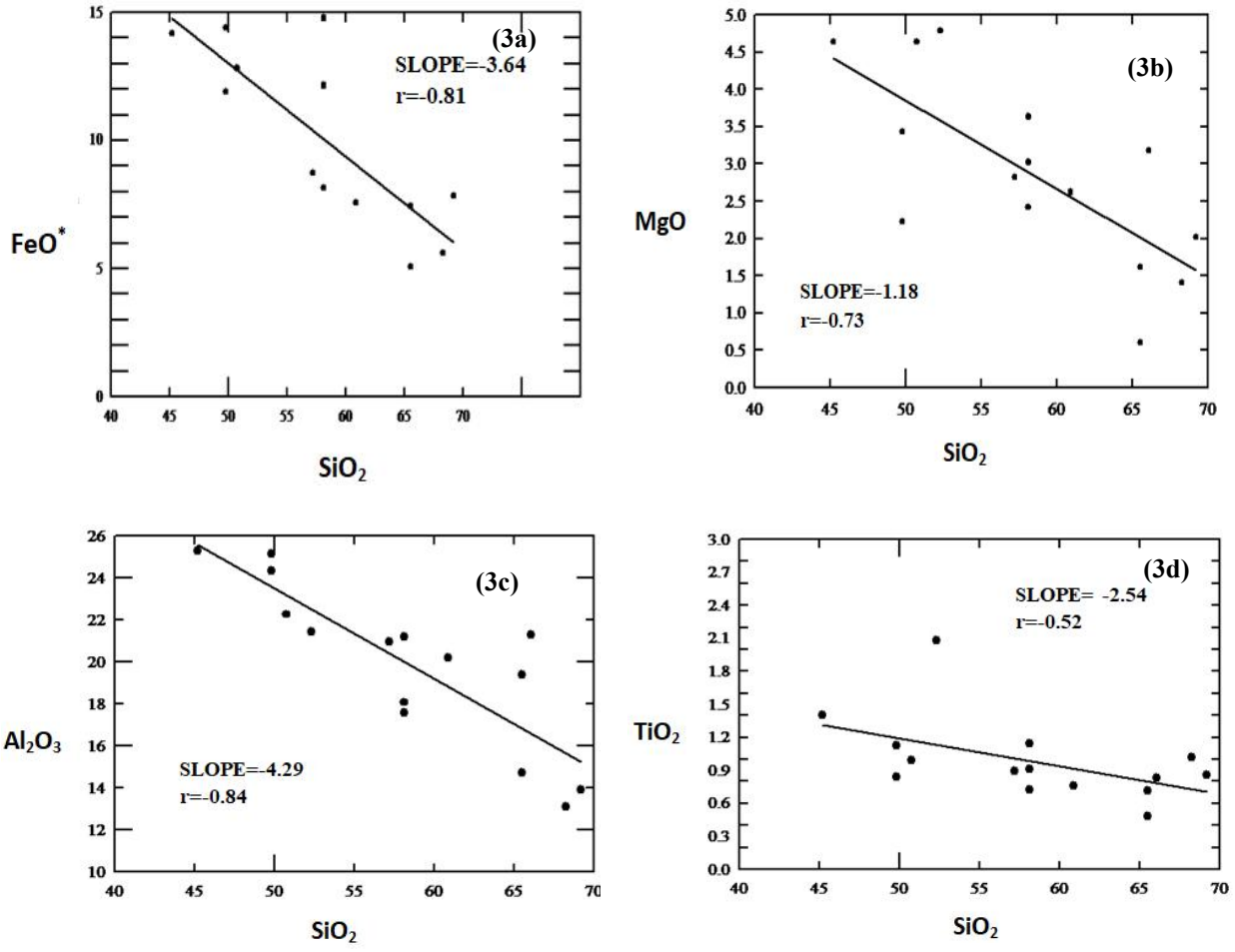

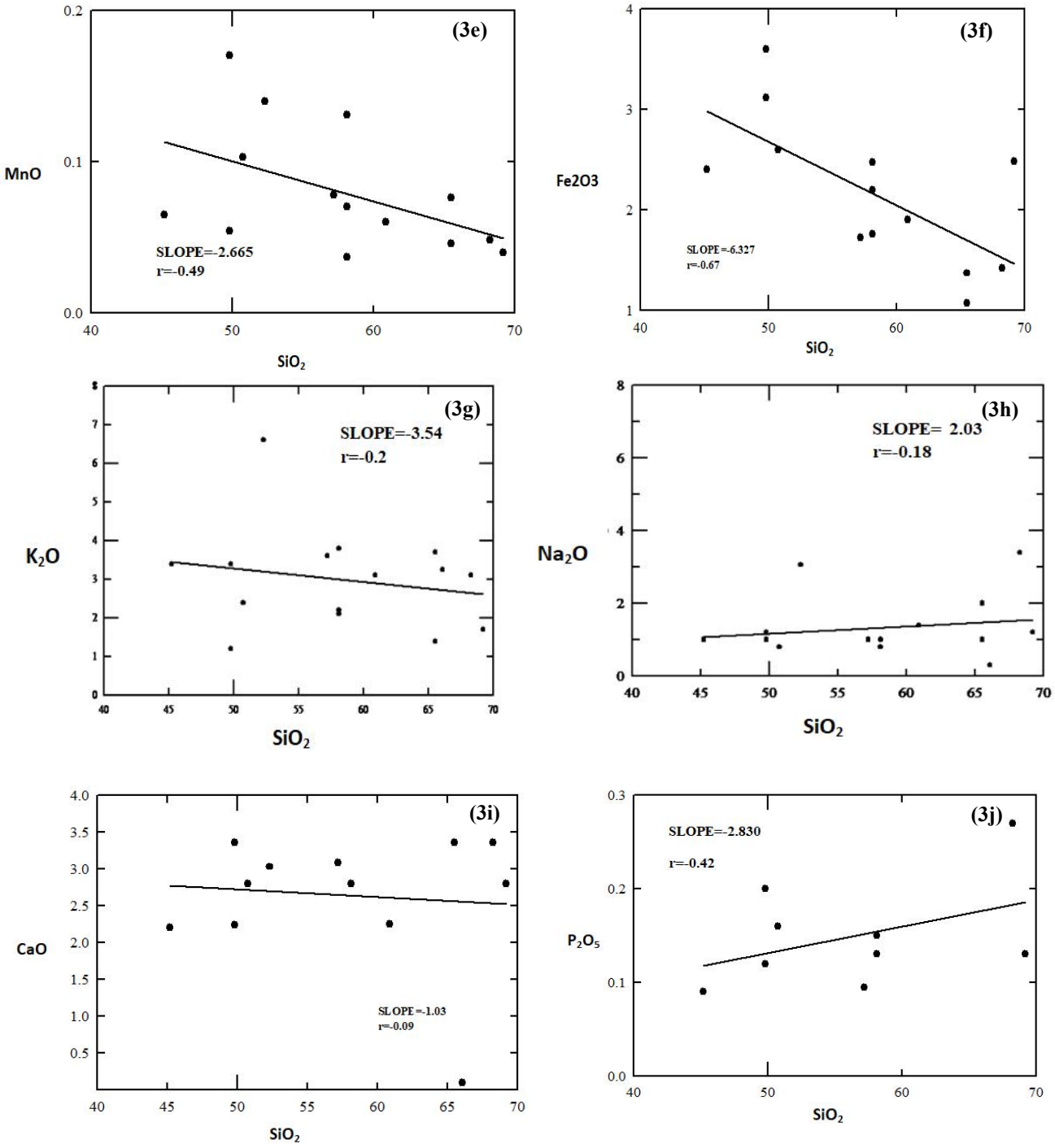

Figure 3. Harker Variation diagrams for Al-rich pelitic granulites/paragneiss from Thana.

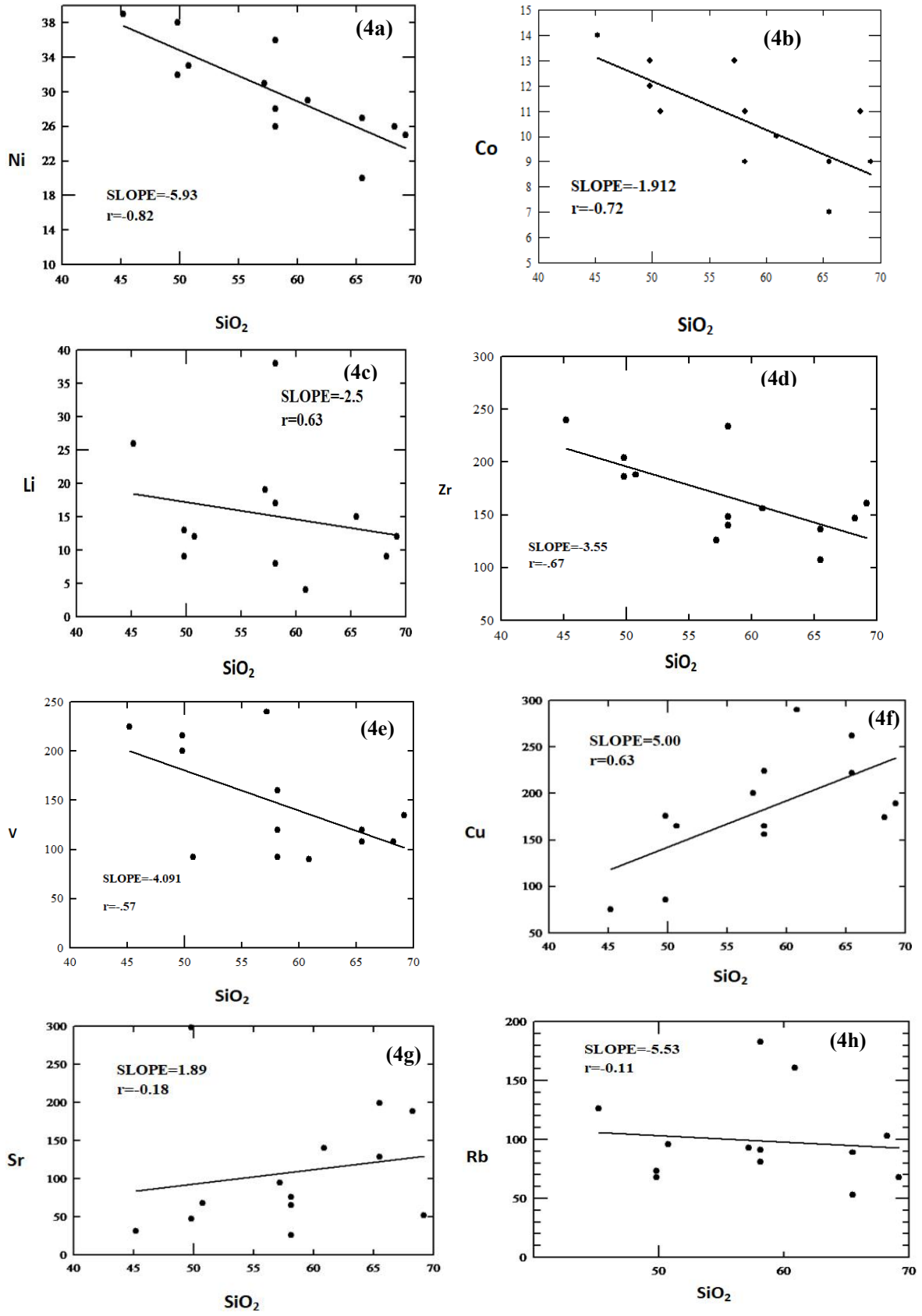

Figure 4. Harker Variation diagrams of SiO_2 verses trace elements for Al-rich pelitic granulites/paragneiss from Thana, Bhilwara, Rajasthan.

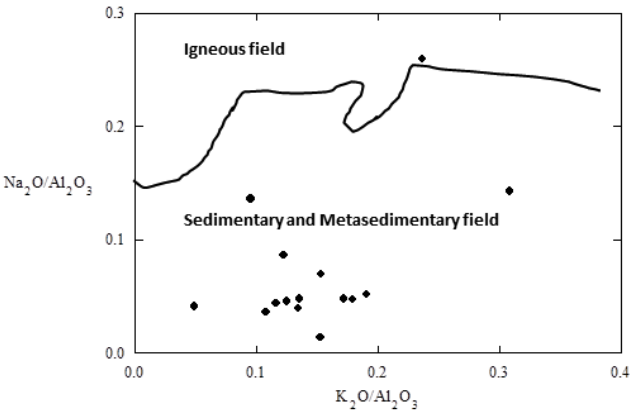

Figure 5. K_2O/Al_2O_3 versus Na_2O/Al_2O_3 after (Garrels and Mackenzie, 1971) for Al-rich pelitic granulites/paragneiss.

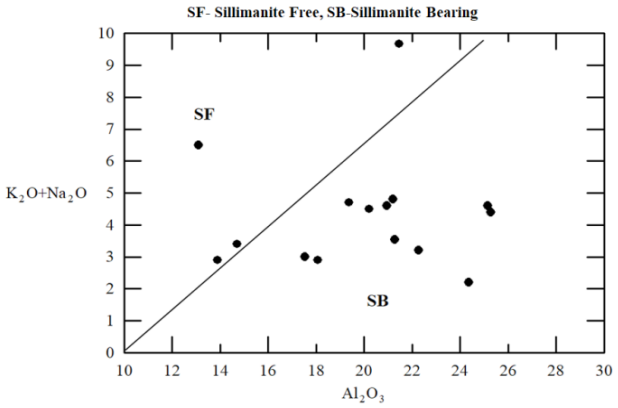

Figure 6. Al_2O_3 against (K_2O + Na_2O) diagram after Goel and Chaudhari, (1979).

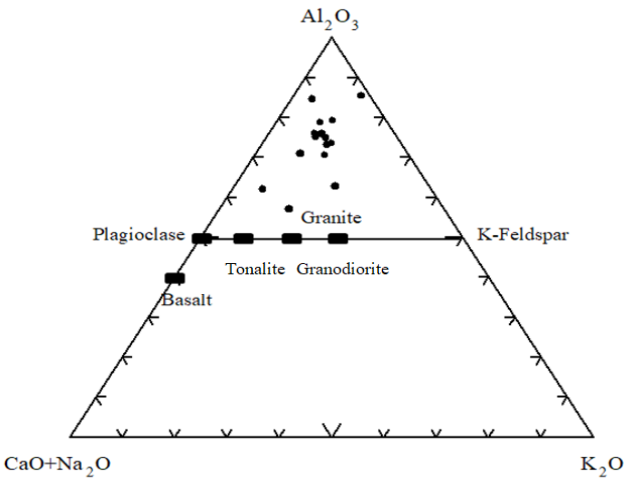

Figure 7. A-CN-K diagram after Nesbitt et al., 2003.

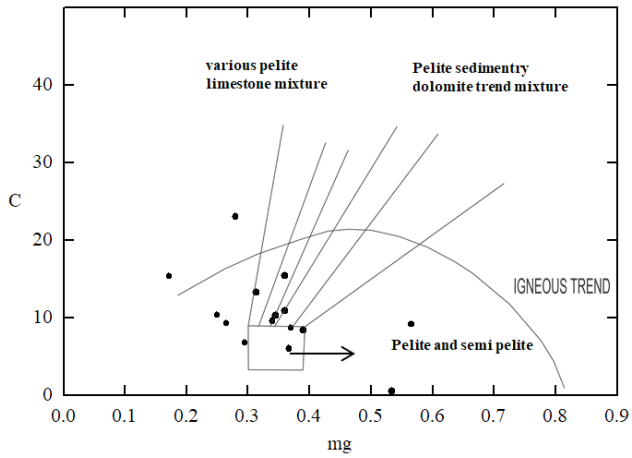

Figure 8. A Niggli mg vs C diagram after Leake (1964) showing plots of rocks from investigated area.

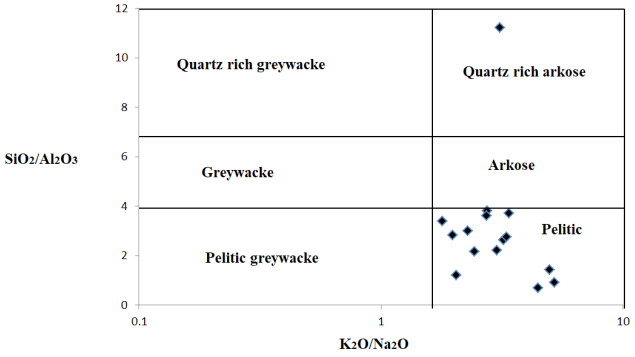

Figure 9. Plot between SiO_2/Al_2O_3 and K_2O/Na_2O for Al-rich pelitic granulites/paragneiss from Thana, Bhilwara, Rajasthan after Wimmenaure (1984) and Condie et al. (1991).

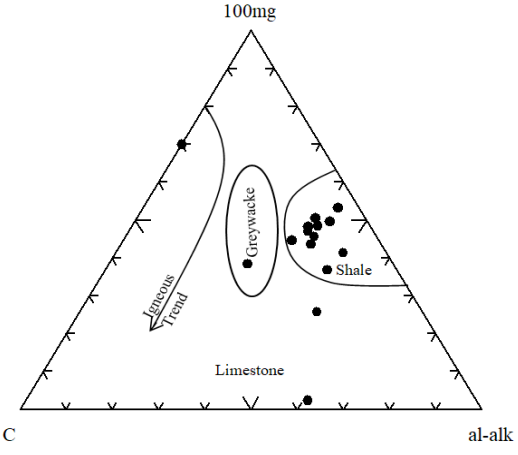

Figure 10. The Niggli 100 mg-c-(al-alk) triangular diagram (Leake, 1964) for Al-rich pelitic granulites/paragneiss from Thana, Bhilwara, Rajasthan.

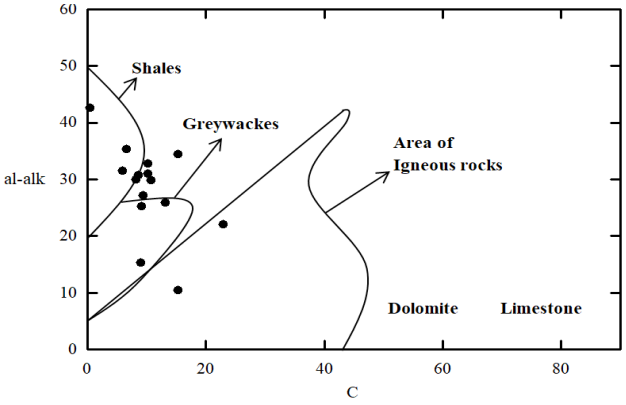

Figure 11. Plot between Niggli c versus (al-alk) values (Leake, 1964) for Al-rich pelitic granulites/paragneiss from Thana, Bhilwara, Rajasthan.

As per Chappel and White, (1974) [32]; Shand, (1943) [33], the A/CNK values of gneisses ranging from 1 to 2.7 support its characterization as strongly peraluminous, S-type source (Figures 12 and 13).

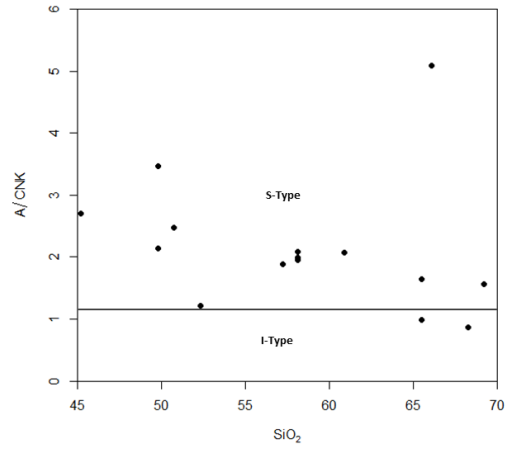

Figure 12. A/NCK vs SiO_2 Plot for Pelitic granulite/Paragneisses after Chappel and White, 1974.

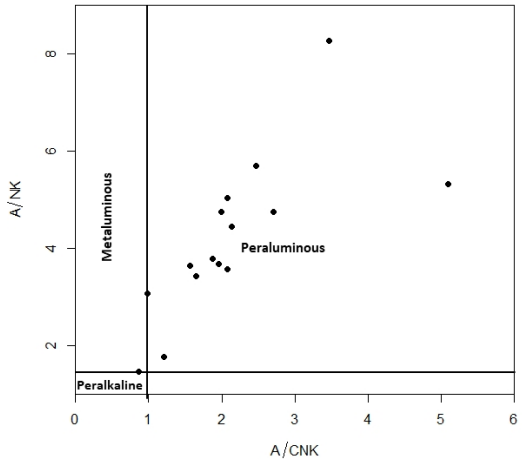

Figure 13. A/NK vs A/CNK Plot for Pelitic granulite/Paragneisses after Shand, 1943.

5. Conclusions

Al-rich pelitic granulites/paragneiss are frequently observed in the medium to high grade metamorphic rocks of Thana. It is dominantly composed of sillimanite-kyanite-garnet-biotite-plagioclase-k-feldspar and a subordinate amount of quartz. Garnet both xenoblastic as well as idioblastic is wrapped round by flaky minerals. Texture is granoblastic to gneissose. Garnet and andalusite occur as porphyroblasts, in a few sections, reaction rims of garnet are present around biotite and kyanite/sillimanite and hornfelsic texture is also observed. Petrographically Al-rich pelitic granulites/paragneiss occupy a substantial portion of the explored area. They are dark, greenish to light in colour and contain garnet, sillimanite, kyanite, staurolite, biotite, K-feldspar, plagioclase, quartz and secondary muscovite and chlorite in several assortments. Garnet is marginally altered into chlorite and, suggests the reaction:

Garnet + fluid = chlorite + quartz + magnetite

The corroded outline of the biotite and its textural relation with fresh garnet and k-feldspar indicate the following reaction.

Biotite + Sillimanite + Quartz = Garnet + K-feldspar + Water

The geochemical plot between SiO_2 vs $Al_2O_3/(CaO + Na_2O + K_2O)$ and A/NK vs A/CNK (Chappell and White 1974) [32] and Shand [33], reflects that Thana pelitic granulite/paragneiss is of S-type and peraluminous in nature. The plot between K_2O/Al_2O_3 and Na_2O/Al_2O_3 Garrels and Machenzie, (1971) [26] and similarly A-CN-K diagram after Nesbitt, et al., (2003) [28] also shows sedimentary field. The chemical variations have also been studied with the help of Niggli values. The 'mg' versus 'c' diagram most of the samples lie in the pelitic and semi-pelite field Leake, (1964) [29] and on the basis of SiO_2/Al_2O_3 versus K_2O/Na_2O diagram Wimmenaure and Fortscher (1984) [30] and Condie, et al., (1991) [31], also indicate sedimentary and metasedimentary fields. Niggli values are also used to examine the nature of the protolith, which strongly support that they are formed by the metamorphism of pre-existing sedimentary rocks. Geochemically, the protolith for these Al-rich pelitic granulites/paragneiss is shale or greywacke.

Author Contributions

This research was conceptualised and interpreted by H. Thomas and Jyoti Bidolya, Aman Soni and Rishabh Batri framed the figures and the manuscript text.

Funding

9/13(687)/94-EMR-I;15/7/94 (CSIR Research Associate Fellowship, New Delhi) to Dr. Harel Thomas.

Data Availability Statement

Samples of paragneiss/Al-rich pelitic assemblages were analyzed at Wadia Institute of Himalayan Geology Dehradun India by Dr. H. Thomas through Atomic absorption spectrometry (AAS) and flame photometry and data is available in Table 1 in paper.

Conflict of Interest

The authors declare that there is no conflict of interests regarding the publication of this article.

Acknowledgement

This research did not receive any specific grant from funding agencies in the public, commercial, or not-for profit sectors. The author (HT) is thankful to Head, Department of Applied Geology and Director, Wadia Institute of Himalayan Geology, Dehradun for providing necessary facilities to carry out this research work. Thanks are given to anonymous referees for their constructive and insightful comments that led to the improvement of this research.

References

[1] Heron, A.M., 1935. The geology of Central Rajputana. Geological Survey of India Memoir. 79, 1-389.

[2] Heron, A.M., 1917. Geology of northern Rajasthan and adjacent districts. Memoir of the Geological Survey of India. 45.

[3] Heron, A.M., 1953. Geology of central Rajasthan. Memoir of the Geological Survey of India. 79.

[4] Gupta, B.C., 1934. The geology of central Mewar. Memoir Geological Survey India, 65, 107-168.

[5] Sarkar, G., Roy Barman, T., Corfu, F., 1989. Timing of continental arc-type magmatism in Northwest India: Evidence from U-Pb zircon geochronology. Journal of Geology. 97, 607-612.

[6] Joshi, M., Thomas, H., Sharma, R.S., 1993. Granulite facies metamorphism in the Archaean gneiss complex from North-Central Rajasthan. Proceedings of the National Academy of Sciences, India. 63(A), 167-187.

[7] Sankara, M.A., Basavalingu, B., Janardhan, A.S., et al., 1994. P-T condition of pelitic granulites and associated charnockites of Chinwali area, west of Delhi fold belt, Rajasthan. Journal of the Geological Society of India. 43, 169-178.

[8] Roy, A.B., Kröner, A., Bhattachaya, P.K., et al., 2005. Metamorphic evolution and zircon geochronology of early Proterozoic granulites in the Aravalli Mountains of northwestern India. Geological Magazine. 142(3), 287-302.

[9] Buick, I.S., Allen, C., Pandit, M., et al., 2006. The Proterozoic magmatic and metamorphic history of the Banded Gneiss Complex, central Rajasthan, India: LA-ICP-MS U-Pb zircon constraints. Precambrian Research. 151(1-2), 119-142.

[10] Rao, C.D., Santosh, M., Purohit, R., et al., 2011. LA-ICP-MS U-Pb zircon age constraints on the Paleoproterozoic and Neoarchean history of the Sandmata Complex in Rajasthan within the NW Indian Plate. Journal of Asian Earth Sciences. 42(3), 286-305.

[11] Sharma, R.S., 1977. Deformational and crystallization history of the Precambrian rocks in north central Aravalli mountain, Rajasthan, India. Precambrian Research. 4, 133-162.

[12] Sharma, R.S., 1988. Patterns of metamorphism in Precambrian rocks of the Aravalli mountain belts. Geological Society of India Memoir. 7, 33-75.

[13] Sharma, R.S., 1999. Crustal development in Rajasthan Craton. Indian Journal of Geology. 71(1&2), 65-80.

[14] Joshi, M., Thomas, H., Sharma, R.S., 1993. Granulite facies metamorphism in the Archaean Complex from North Central Rajasthan. Proceedings of the National Academy of Sciences, India. 63(A), I, 167-187.

[15] Thomas, H., 1995. Pressure-Temperature considerations for granulites from Thana Gyangarh, Distt. Bhilwara, Rajasthan: Implications for crustal evolution. Magmatism in Relation to Diverse Tectonic settings. Oxford & IBH Publishing Co. Pvt. Ltd. pp. 439-456.

[16] Thomas, H., 2005. Polymetamorphism in the archaean gneiss complex of Shivpura Gyangarh District Bhilwara, Rajasthan. Granulite facies metamorphism and crustal evolution. Atlantic Publishers & Dist: New Delhi. pp. 123-147.

[17] Thomas, H., Sujata, S., 2008. Petrology and reaction texture of the Meta-Norites from Shivpura, Bhilwara District, Rajasthan. Indian dykes geochemistry, geophysics and geochronology. Narosa Publishing House Pvt. Ltd.: Ballygunge. pp. 571-587.

[18] Thomas, H., Vishwakarma, N., 2011. Petrochemical studies of amphibolites from Kirimal district Bhilwara, Rajasthan, India. Memoir of the Geological Society of India. 77, 559-571.

[19] Thomas, H., Vishwakarma, N., 2011. Geochemical characters of amphibolites from Asind District Bhilwara, Rajasthan, India. Asian Journal of Chemistry. 25(12), 5433-5440.

[20] Thomas, H., Paudel, L., 2015. Petrogeochemistry of amphibolites from Shivpura District Bhilwara,

Rajasthan, India. Journal of Institute of Science and Technology. 20(2), 103-112.
DOI: https://doi.org/10.3126/jist.v20i2.13962

[21] Kavita, S., Thomas, H., 2018. Petrogeochemistry of gneissic rocks exposed around Arjungarh, District Rajsamand, Rajasthan, India. Crimson Publishers. 3(3), 85-91.

[22] Vishwakarma, N., Thomas, H., 2015. Petrological and geochemical characteristics of charnockite from Asind, District-Bhilwara Rajasthan: Implication for its origin. Journal of Applied Geochemistry. 17(1), 10-21.

[23] Thomas, H., Rana, H., 2020. Mineral chemistry and nomenclature of amphiboles from Thana Bhilwara, Rajasthan, India. Journal of Geological Research. 2(2), 34-40.
DOI: https://doi.org/10.30564/jgr.v2i2.2130

[24] Gupta, S.N., Arora, Y.K., Mathur, R.K., et al., 1980. Lithostratigraphic map of Aravalli Region (1:1000,000). Memoir of the Geological Society of India, Calcutta.

[25] Gupta, S.N., Arora, Y.K., Mathur, R.K., et al., 1997. The Precambrian geology of the Aravalli Region, Southern Rajasthan and northeastern Gujarat. Memoir of the Geological Society of India. 123, 262.

[26] Garrels, L.M., Machenzie, F.T., 1971. Evolution of sedimentary rocks. Norton Inc.: New York. pp. 307.

[27] Goel, O.P., Chaudhari, M.W., 1979. Evolution of sedimentary rocks: New York, Lithos. 11, 153-158.

[28] Nesbitt, S.W., Edward, J.Z., 2003. The diurnal cycle of rainfall and convective intensity according to three years of TRMM measurements. Journal of Climate. 16(10), 1456-1475.

[29] Leake, B.E., 1964. The chemical distinction between para and ortho amphibolite. Journal of Petrology. 5, 238-254.

[30] Wimmenaure, W., 1984. Das prävariskische Kristalline im Schwarzwald. 62(2), 69-86.

[31] Condie, K.C., Wilks, M., Rosen, D.M., et al., 1991. Geochemistry of metasediments from Precambrian Hapschan Series, Eastern Anabar Shield, Siberia. Precambrian Research. 50, 37-47.

[32] Chappel, B.W., White, A.J.R., 1974. Two contrasting granite types. Pacific Geology. 8(2), 173-174.

[33] Shand, S.J., 1943. Eruptive rocks. Their genesis, composition, classification, and their relation to ore-deposits with a chapter on meteorite, 2nd edition. John Wiley & Sons: New York. pp. 1-444.

Earth and Planetary Science
https://ojs.nassg.org/index.php/eps/index

RESEARCH ARTICLE

New Five Southern Tethyan Agglutinated Foraminiferal Species

Haidar Salim Anan *

Al Azhar University-Gaza, P.O Box 1277, Gaza, Palestine

ARTICLE INFO

Article history
Received: 27 June 2022
Revised: 13 September 2022
Accepted: 3 January 2023
Published Online: 16 February 2023

Keywords:
Foraminifera
Campanian
Paleogene
Paleogeography
Egypt
Iraq
Iran
Southern Tethys

ABSTRACT

Benthic foraminifera was studied as part of an investigation of the Dababiya section (Egypt), which was undertaken to document a candidate section for the Global Stratotype Section and Point (GSSP) for the base of the Ypresian Stage, Thanetian/Ypresian boundary, Late Campanian Dokan and Azmer sections of Kurdistan (NE Iraq), and the type section of Khangiran Formation of Khangiran section (NE Iran). Five new species of the genera *Pseudogaudryina* and *Pseudogaudryinella* are proposed, from three countries Egypt, Iraq and Iran, and from Campanian and Ypresian sediments. Three species of *Pseudogaudryina: P. dababiyaensis* (from Egypt), *P. kurdistanensis* and *P. iraqensis* (from Iraq), two species from Iran: *Pseudogaudryinella iranica* and *Pseudoclavulina iranica*. The Tethyan continental shelf fauna Midway-Type Fauna (MTF) of deep middle neritic to the upper bathyal environment is interpreted.

1. Introduction

The present study aims at throwing light on: 1) the stratigraphy and taxonomy of new five members of the genera *Pseudogaudryina* (*dababiyaensis*, *kurdistanensis* and *iraqensis*), *Pseudogaudryinella iranica* and *Pseudoclavulina iranica*, 2) the paleogeographic distribution of them in many localities in the Southern Tethys: Iran, Iraq, Jordan and Egypt (Figure 1). This wide geographic distribution of these taxa indicates that the ancestral Tethys was open and connected with the ancestral Indian Ocean (e.g., Aubert, & Berggren [1]; Morsi et al. [2]; Salahi [3]).

2. Systematic Paleontology

The taxonomy of Kaminski [4] is followed in this study for three members of the genus *Pseudogaudryina* Cushman, another species of the genus *Pseudogaudryinella* Cushman, and one species of the genus *Pseudoclavulina* Cushman. The stratigraphic positions are also presented. Modern references have been added to complete the descriptions of the recorded species (Plate 1).

*Corresponding Author:
Haidar Salim Anan,
Al Azhar University-Gaza, P.O Box 1277, Gaza, Palestine;
Email: profanan@gmail.com

DOI: http://dx.doi.org/10.36956/eps.v1i2.569

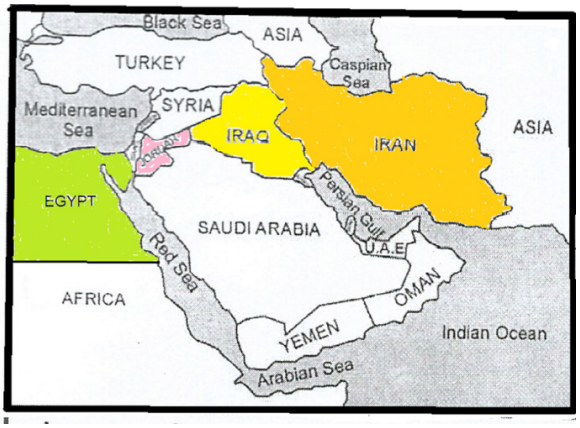

Figure 1. Location map of the three countries (Egypt, Jordan, Iraq and Iran) in the Southern Tethys.

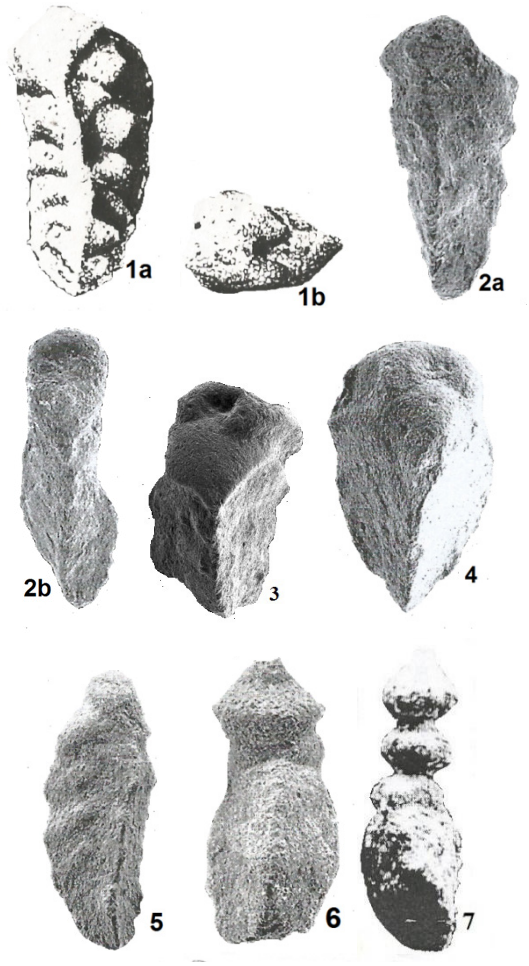

Plate 1. Figure 1a,b. *Pseudogaudryina atlantica* Bailey [5], type species, 1a. side view, 1b. apertural view x 80; 2a,b. *P. dababiyaensis* Anan, n. sp., 2a. side view, 2b. side view x 85; 3. *P. kurdistanensis* Anan, n. sp., apertural view x 85; 4. *P. iraqensis* Anan, n. sp., side view x 85; 5. *Pseudogaudryinella iranica* Anan, n. sp., side view x 80; 6. *Pseudoclavulina iranica* Anan, n. sp., side view x 70; 7. *P. futyani* Anan [6], side view x 40.

Genus *Pseudogaudryina* Cushman, 1936

Remarks: The type species (Plate 1, Figure 1) is triangular throughout the agglutinated test with an early tri-serial stage and later biserial. The two series of angular biserial chambers are dissimilar, one series being roughly triangular in section and the other quadrangular in section maintaining the triangular test shape, aperture an interiomarginal arch (Leoblich & Tappan [7]).

***Pseudogaudryina dababiyaensis* Anan, n. sp.** (Plate 1, Figure 2a,b (= *Gaudryina* sp. Alegret & Ortiz [8], p. 442, Plate 1, Figure 2a,b).

Holotype: Illustrated specimen in Plate 1, Figure 2a,b.

Diameter of the holotype: Length 0.88 mm, width 0.44 mm.

Etymology: After the site of the Paleocene/Eocene Boundary Global Stratotype (Egypt).

Type locality: Dababiya section, south Luxor (Figure 2).

Age: Early Ypresian, *P. wilcoxensis* Zone (E2).

Diagnosis: This species has a triangular agglutinated test with tri-serial early stage and later biserial, one end of the biserial has a pointed end, while the periphery of the other end is rounded, aperture wide interiomarginal arch. It has a wide triangular tri-serial portion, while the biserial has parallel edges.

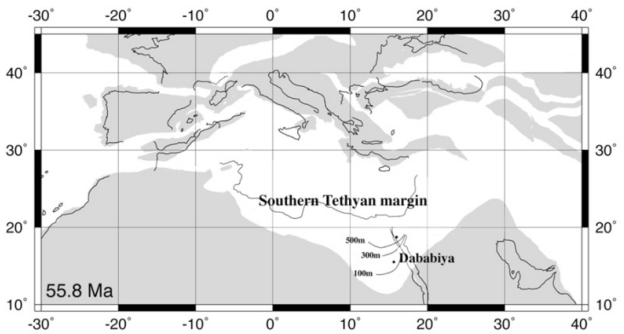

Figure 2. Location map of the Dababiya section (Egypt) in the Southern Tethys (after Alegret & Ortiz [8]).

***Pseudogaudryina iraqensis* Anan, n. sp.** (Plate 1, Figure 4) (= *Gaudryina pyramidata* Cushman - Jaff & Lawa [9], p. 14, Plate 2, Figure 7, *non* Figures 5,6.

Holotype: Illustrated specimen in Plate 1, Figure 4.

Diameter of the holotype: Length 0.96 mm, width 0.48 mm.

Etymology: After the Republic of Iraq.

Type locality: Shiranish Formation, Dokan section (Figure 4).

Age: Late Campanian.

Diagnosis: This species has a triangular throughout the fine-grained agglutinated test with tri-serial early stage and later biserial, and one end of the biserial has a pointed

end, while the outline of the other end is rounded, regular edges of the test, aperture wide interiomarginal arch. This species differs from the *P. iraqensis* in its wider width of the test, regular periphery than irregular, and less tapering pointed end of the prefinal biserial chamber.

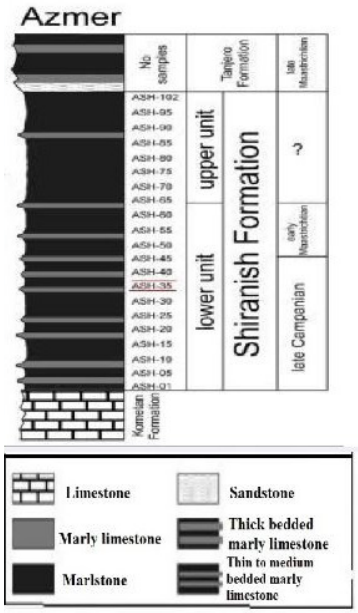

Figure 3. Stratigraphic log of the Azmer section, Kurdistan region (NE Iraq) including the position of the sample-ASH-35, the type locality of P. *kurdistanensis*, (for the lithological description see the next figure 4, after Jaff & Lawa [9]).

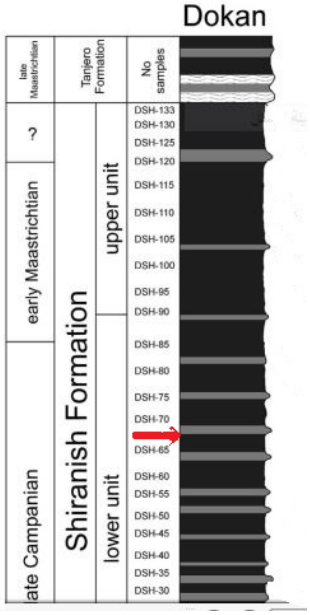

Figure 4. Stratigraphic log of the Dokan section, Kurdistan region (NE Iraq) including the position of the sample-DSH-68, the type locality of *Pseudogaudryina iraqensis* (after Jaff & Lawa [9]).

Genus *Pseudogaudryinella* Cushman, 1936

***Pseudogaudryinella iranica* Anan, n. sp.** (Plate 1, Figure 5) (= *Gaudryina* sp. Salahi [3], p. 314, Plate 4, Figure 23, *non* Figure 28.

Holotype: Illustrated specimen in Plate 1, Figure 5.

Diameter of the holotype: Length 0.92 mm, width 0.34 mm.

Etymology: After the Islamic Republic of Iran (Figure 5).

Type locality: Ypresian.

Diagnosis: Test elongate, early-stage tri-serial triangular in section, followed by biserial, and finally uniserial rounded in section, aperture rounded terminal on the short neck in the last chamber. This species differs from *Pseudogaudryinella iraqensis Anan* [6], by its longer and irregular tri-serial portion, and lesser size of the uniserial final chamber.

Figure 5. The type section of Khangiran Formation, Kopet-Dagh Basin, NE Iran (after Salahi [3]).

Genus *Pseudoclavulina* Cushman, 1936

***Pseudoclavulina iranica* Anan (n. sp.)** (Plate 1, Figure 6) (= *Gaudryina* sp. Salahi [3], p. 314, Plate 4, Figure 28, *non* Figures 14,23.

Holotype: Illustrated specimen in Plate 1, Figure 6.

Diameter of the holotype: Length 0.80 mm, width 0.34 mm.

Etymology: After the Islamic Republic of Iran.

Type locality: The Islamic Republic of Iran.

Age: Late Campanian.

Diagnosis: This species has a large tri-serial part and comprise ⅔ of the fine-grained agglutinated test, followed by two chambers of the flask-shaped uniserial portion, rounded terminal aperture on a short neck, and deep sutures. This Iranian species differs from the Jordanian species *P. futyani* Anan in its larger tri-serial part and lesser numbers of the uniserial part.

***Pseudoclavulina futyani* Anan** [6] (Plate 1, Figure 7)

(= *Clavulina barnardi* Futyan [10], p. 522, Plate 81, Figure 4, *non* Figure 3.

Remarks: This Paleocene species has a large tri-serial part and comprise one-half of the test, the uniserial part has slightly irregular rectilinear three flask-shaped inflated chambers, a rounded terminal aperture at the end of the tubular neck, and deeply excavated sutures. *Pseudoclavulina futyani* differs from *P. barnardi* (Futyan) in its larger tri-serial portion of *futyani* of ½ of the entire test instead of ¼ in *barnardi*, and also three uniserial chambers in the former instead of five to eight chambers in the latter. *P. futyani* is, so far endemic to Jordan.

3. Paleogeography

The five new agglutinated benthic foraminiferal species were originally identified and erected in three countries in the Southern Tethys: Egypt, Iraq and Iran. The Tethys Ocean had connected with the Atlantic Ocean in the west and extended across the modern Mediterranean Sea to the Indian Ocean in the east, during the Campanian through Paleogene times (Figure 6).

Figure 6. The Tethys Ocean in the Early Paleogene, showing the location of Africa, India, Asia and Europe (after Salahi [3]).

4. Paleoenvironment

The five recorded species are endemic to their original localities from Egypt, Iraq and Iran. Most of the identified species in the Southern Tethys (Tunisia, Egypt, Jordan, UAE, Pakistan, Figure 7) by many authors are related largely to Midway Type Fauna "MTF" (deep middle neritic to the upper bathyal environment). The Middle East basins show possible migration routes during the Campanian-Ypresian times (LeRoy [11], Haque [12], Berggren & Aubert [13], Futyan [10], Anan [14]). On the other hand, the Shiranish Formation has been classically interpreted as a succession of deep-water deposits (Jaff & Lawa [9]).

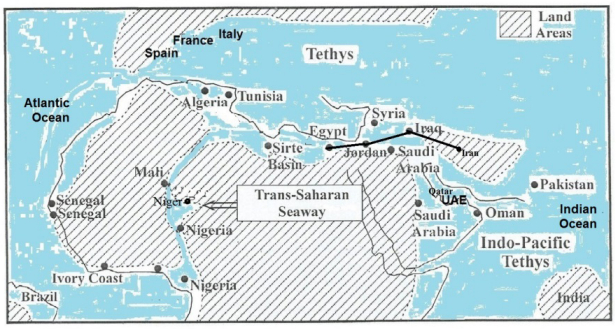

Figure 7. The paleogeographic map of the Southern Tethys around the KPg boundary: Egypt, Jordan, Iraq and Iran (after Morsi et al. [2]).

Conflict of Interest

There is no conflict of interest.

Acknowledgement

Gratitude expressed to the editor of the Earth and Planetary Science, the unknown reviewers for their valuable comments, and also to my daughter Dr. Huda H. Anan for her help in the development of the figures and plate.

References

[1] Aubert, J., Berggren, W.A., 1976. Paleocene benthonic foraminiferal biostratigraphy and paleoecology of Tunisia. Bulletin du Centre de Recherches Pau-SNPA. 10(2), 379-469.

[2] Morsi, A.M., Faris, M., Zalat, A., et al., 2008. Maastrichtian-Early Eocene ostracodes from west-central Sinai, Egypt-taxonomy, biostratigraphy, paleoecology and paleobiogeography. Revue de Paléobiologie. 27(1), 159-189.

[3] Salahi, A., 2021. Late Paleocene-Middle Eocene planktonic and mall benthic foraminiferal fauna from the Khangiran Formation, Kopet-Dagh Basin (NE Iran), Southernmost Peri-Tethys. Stratigraphy and Geological Correlation. 29(3), 303-321.

[4] Kaminski, M.A., 2014. The year 2010 classification of the agglutinated foraminifera. Micropaleontology. 60(1), 89-108.

[5] Bailey, J.W., 1851. Microscopical examination of soundings made by the U.S. coast survey off Atlantic coast of the U.S. Smithsonian Contributions to Knowledge. 2, 1-15.

[6] Anan, H.S., 2022. Contribution to the paleontology, stratigraphy and paleogeography of ninety-seven Southern Tethyan agglutinated foraminiferal species. Earth and Planetary Science. 1(1), 22-34.

[7] Loeblich, A.R., Tappan, H., 1988, Foraminiferal genera and their classification. Springer: German. Part 1, p. 970. Part 2, p. 847.

[8] Alegret, L., Ortiz, S., 2006/2007. Global extinction event in benthic foraminifera across the Paleocene/Eocene boundary at the Dababiya Stratotype section. Micropaleontology. 52, 433-447.

[9] Jaff, R.B.N., Lawa, F.A., 2019. Palaeoenvironmental signature of the Late Campanian-Early Maastrichtian benthonic foraminiferal assemblages of Kurdistan, Northeast Iraq. Journal of African Earth Sciences. 1-21.

[10] Futyan, A.I., 1976. Late mesozoic and early cainozoic benthonic foraminifera from Jordan. Palaeontology. 19(3), 53-66.

[11] LeRoy, L.W., 1953. Biostratigraphy of Maqfi section, Egypt. Geological Society of American Memoir. 54, 1-73.

[12] Haque, A.F.M.M., 1956. The foraminifera of the Ranikot and the Laki of the Nammal Gorge, Salt Range, Pakistan. Pakistan Geological Survey Memoir, Palaeontologica Pakistanica. 1, 1-229.

[13] Berggren, W.A., Aubert, J., 1975. Paleocene benthonic foraminiferal biostratigraphy, paleobiogeography and paleoecology of Atlantic-Tethyan regions: Midway-type fauna. Palaeogeography, Palaeoclimatology, Palaeoecology. 18, 73-192.

[14] Anan, H.S., 2016. Early Paleogene agglutinated foraminifera from the Middle East (Egypt and Arabia) and its distribution in the Tethys. Spanish Journal of Paleontology. 31(2), 353-368.

Earth and Planetary Science
https://ojs.nassg.org/index.php/eps/index

REVIEW ARTICLE

An Overview of Stratospheric Ozone and Climate Effects

M.M. Karadan[1] P.V.S. Raju[1*] P.C.S. Devara[2]

1. Centre for Ocean Atmospheric Science and Technology, Amity University Rajasthan, Kant Kalwar, Jaipur, Rajasthan, 303002, India
2. Centre of Excellence in Ocean-Atmospheric Science and Technology & Environmental Science and Health, Amity University Haryana, Gurugram, Haryana, 122413, India

ARTICLE INFO

Article history
Received: 30 November 2022
Revised: 14 February 2023
Accepted: 28 February 2023
Published Online: 9 March 2023

Keywords:
Ozone layer depletion
Greenhouse gases
Chlorofluorocarbons
Ozone depleting substances
Montreal protocol

ABSTRACT

Anthropogenic Chlorofluorocarbons (CFCs) compelled stratospheric ozone reduction is one of the significant global environmental issues of this era. Ozone acts as a life saviour in the stratosphere whereas the same plays a role as a secondary air pollutant at tropospheric levels. This review encompasses studies involving the science of ozone destruction with an emphasis on chemical processes involved, minimum ozone features, ozone hole area characteristics, various Ozone Depleting Substances (ODSs), consequences of reduced stratospheric ozone levels, and the different executed international commitments to restrain ozone depletion. It has been perceived that the decrease in stratospheric ozone volume gives away extensively to climate change such as through ozone chemistry fluctuations of polar annular modes and its Greenhouse Gas (GHG) features. Different international ozone layer protection agreements have been performing a major role in limiting stratospheric ozone depletion thereby its adverse effects, and specifically Montreal protocol has been a great success to this point.

1. Introduction

Ozone, the triatomic allotrope of oxygen (chemical formula: O_3) is a chemical entity that is much less stable than its diatomic form O_2. It is colourless, odourless gas at considerable concentrations. It exists as a pale blue gas at high concentrations which are weakly soluble in water and easily soluble in inert non-polar solvents. Also, ozone condenses to form a dark blue liquid at a temperature of –112 °C. Throughout the Earth's atmosphere, ozone is present only in slight concentration and it makes up only 0.6 ppm of the entire atmosphere by volume. The chief irony is that ozone plays as a life saviour over the stratosphere whereas in the troposphere it acts as a secondary air pollutant. Around 90% of Earth's atmospheric ozone comes from the lower-mid stratosphere, that is in between 15 km and 35 km altitude (Figure 1) [1]. The rest 10% is only found at the tropospheric level [1,2]. The large-scale

*Corresponding Author:
P.V.S. Raju,
Centre for Ocean Atmospheric Science and Technology, Amity University Rajasthan, Kant Kalwar, Jaipur, Rajasthan, 303002, India;
Email: pemmani@gmail.com

DOI: http://dx.doi.org/10.36956/eps.v1i2.782

quasi-horizontal exchange phenomena have a great contribution to making up the intricate vertical distribution of ozone [3]. Unlike the middle and high latitudes, the lower latitudes exhibit a less pronounced association of upper atmospheric waves with diurnal ozone variations [4].

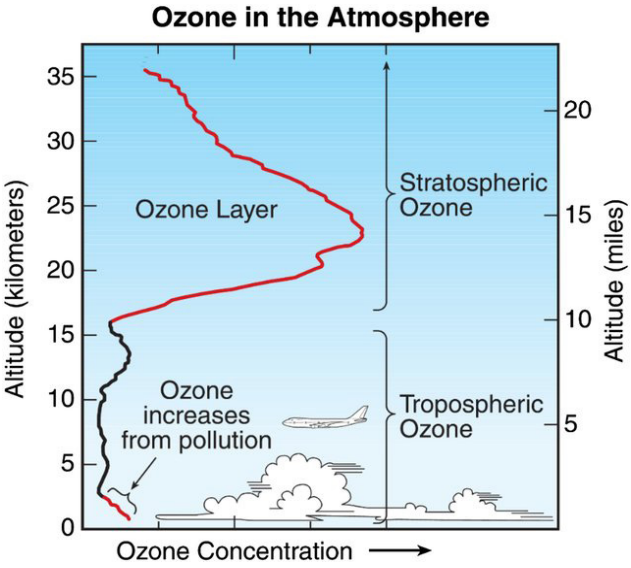

Figure 1. Vertical characteristics of ozone in Earth's atmosphere. Ozone concentration maximum is found at 23 to 25 km. And a tropospheric local maximum is noted at surface level which is attributed by pollution [1].

A slight hike of ozone in the near-surface layer occurs as a consequence of anthropogenic emissions. Between 15 km and 35 km altitudes, a prolific amount of ozone is seen, and of which is present with maximum abundance at the 23 km to 25 km region. Therefore, the same region is often termed as an ozone layer [1,5]. It acts as a shielding layer for Earth from injurious solar Ultraviolet (UV) radiation effects. Even with energy-weak UV radiation, ozone gets split into molecular oxygen and free atomic oxygen. The production of atmospheric ozone is seriously connected with the dynamic equilibrium between ozone and oxygen. This equilibrium nowadays is badly affected by anthropologic halocarbon emissions. Human-induced surface ozone emissions make air polluted in the troposphere [6]. On a multi-annual temporal scale, extra-polar lower stratospheric ozone is regulated by distinct atmospheric dynamic processes [7]. By the manifestation of various photochemical reactions, maximum ozone mixing ratios are observed in the tropical middle stratosphere [1]. And that the maximum stratospheric ozone mixing ratio is present only in the range of ten molecules per one million air molecules. Nonetheless, it has found a profound significance in life on Earth. Also, there exists an assumption that the evolution of life on Earth became possible only after the set-up of the atmospheric ozone layer [1]. The biologically detrimental Ultraviolet-B (UV-B) radiations are largely absorbed by stratospheric ozone and thus the ozone layer care for life forms and various ecosystems on Earth [8]. The major objective of the article is to understand the stratospheric ozone condition under certain international commitments and evaluate it with its current circumstances. Also, the anthropogenic impression of the stratospheric ozone concentration will be examined along with some powerful chemical and dynamical processes involved in changing stratospheric ozone abundance.

The annual worldwide casualties affected by air pollution are over 6 million, which is far more than that of AIDS, Malaria, and Tuberculosis combined. Surface ozone is a Greenhouse Gas and a major pollutant harmful to humans, crops, and ecosystem productivity [9-13]. And it is not emitted straightaway. Instead it is produced by nitrogen oxide (NO_X) chemical reactions and by Volatile Organic Compounds (VOCs) [9]. It is observed that a significant part of anthropogenic emission contribution has shifted from Europe and North America to Asian countries like India, China, the Republic of Korea, and Japan [14-17]. Furthermore, across these countries, surface emissions only dominate in the tropospheric ozone variations (Wang Wei-Chyung and Tanaka 2009). Surface ozone levels are found to be high in rural regions as there is forest agricultural production, and water supply [18]. Thus, their ozone production causes injuriously over ecosystems with effects like plant toxicity, cell damage, impacts on individual organisms, their ecological interactions, and effects on chemical and biological processes [14,19]. Superabundant intake of ozone can cause physiological alterations in photosynthesis, respiration, carbon allocation, stomatal functioning, and on volatile organic compound emissions. Also, it gives rise to growth reduction, seed production cutback, intensified senescence, and varied vulnerability toward biotic and abiotic stresses [14,20]. More extended ozone intake by plants can bring alteration in gene expression, species composition, and carbon sequestration [21]. Excessive exposure to ozone is capable of bringing leaf stipples, and leaf lesions [22].

2. Ozone Measurement Techniques

A corporal foundation for the development of optical estimation of ozone started in the second half of the nineteenth century. In 1920, Fabry and Buisson reported daily measurements of ozone effectively for the first in history by comparing wavelength parameters of sunlight with different intensities [23]. Afterward, several instruments came into the field of ozone measurement including electrochemical Ozonesondes [24,25]. Balloon-borne Ozonesondes have been carrying a significant role in measuring and

verifying ozone and ozone-depleting chemicals [26].

The aggregate quantity of ozone present in a column that vertically extends from the Earth's surface up to the upper layer of the atmosphere is called Total Column Ozone (TCO). This can be calculated by ground-based and satellite measurement systems. These are reported in Dobson Units (DU). This unit can be defined as, "all the ozone over a confined volume is compressed down to a temperature of 0 °C and a pressure of 1 atm (STP), then it forms an ozone block of 3 mm thickness which is considered to be equal to 300 DU ozone" [27].

2.1 Dobson Spectrophotometer

In 1924, the British meteorologist Gordon Miller Dobson invented an ozone-measuring instrument called a Dobson spectrophotometer or simply a Dobson spectrometer. This instrument comprises a double quartz-prism monochromator which allows simultaneous measurements at two wavelengths over the UV region (Figure 2) [28]. At these two wavelengths the absorption rates will be different [29]. So this instrument measures a series of wavelength pairs [28]. And the Total Column Ozone (TCO) estimation is done by comparing the absorption of each pair of wavelengths. The final TCO can be determined by finding the weighted mean average of individual estimates. The double pair wavelengths can be utilised for the assessment, i.e., 305.5/325.4 and 317.6/339.8 nm [30].

Bass-Paur ozone absorption coefficients are utilized for the estimation [31]. The two circumstances to be taken care of when performing individual observations are: (i) looking at the direct sun in a clear sky, and (ii) measuring Solar Zenith Angle (SZA) should be less than 84° [32]. The total evaluated error of Dobson spectrometer measurements was found to be 3% [33].

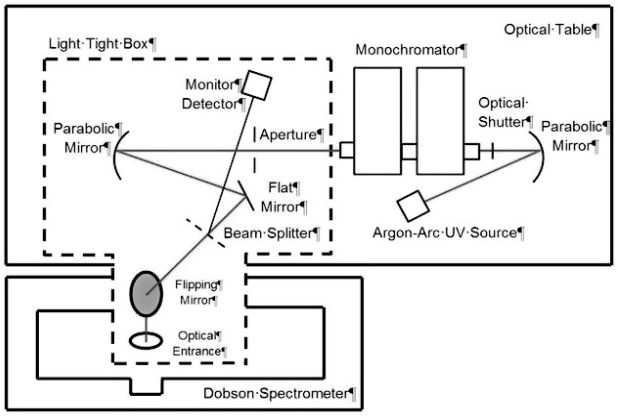

Figure 2. A schematic diagram of Dobson spectrophotometer [28].

2.2 Brewer Spectrophotometer

This instrument follows an analogous working principle to Dobson spectrophotometer to find out TCO (Figure 3) [34]. It comprises a focal plane mounted with five highly precise exit slits accompanied by a single diffraction grating. These slits are optimised for the assessment of ozone and SO_2 which are respective to five wavelengths namely 306.3 nm, 310.1 nm, 313.5 nm, 316.0 nm, and 320.0 nm. A Fabry lens is also placed after the exit slits through which a reduced image of a diffraction grating is produced on a 10 mm diameter photocathode of a photomultiplier tube. The sequential experimentation is carried out by moving a mask in front of each slit. When the slits are kept static, a stable wavelength calibration is achieved [34]. The instrumental resolution of the Dobson spectrometer was found to be in the range between 0.9 nm and 3.0 nm whereas the Brewer instrument has a much better resolution of 0.6 nm [35].

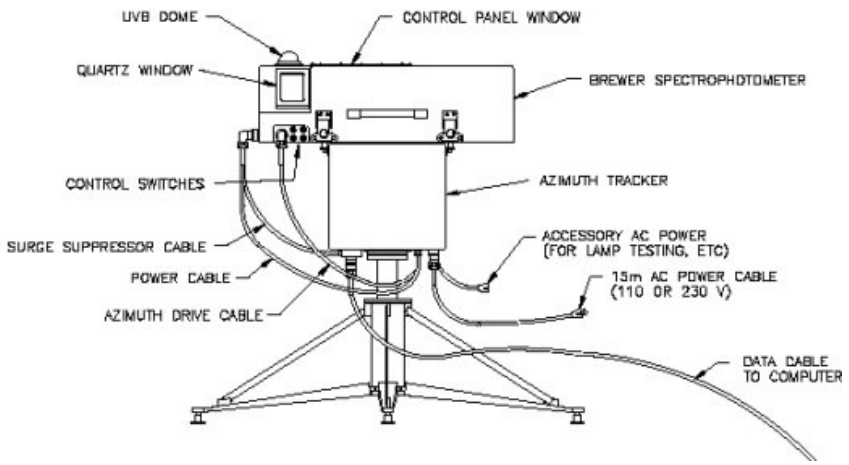

Figure 3. An experimental arrangement of Brewer spectrophotometer [34].

2.3 SAOZ (System D'Analyse Par Observations Zenithales)

It is an UV-visible spectrometer with a resolution of 1 nm in that the observation is taken looking at sunlight scattered at Zenith during the dusk time. The ozone's Chappuis absorption (450-650 nm) is assessed by the instrument at an SZA between 86° and 91° [36,37]. As SAOZ instruments are capable of performing observations in visible wavelength range, the same are capable of undertaking measurements throughout the year [38]. As the air-mass factor is considered in retrieving observations, the error is found to be 3% and it may be higher in ozone-hole circumstances [39].

2.4 Differential Optical Absorption Spectrometer (DOAS)

This is a similar kind of instrument as SAOZ in which both UV and Visible channels are present in the spectrograph. And the ozone estimations are undergone at 490-555 nm wavelength range and at an SZA between 84° and 90°. This method brings an accuracy of 2% [40].

2.5 Satellite Measurements

In addition to the ground-based measurements, there exist many artificial satellites for measuring columnar ozone and retrieving data; namely Total Ozone Mapping Spectrometer (TOMS), Ozone Monitoring Instrument (OMI), Global Ozone Monitoring Experiment (GOME), Microwave Limb Sounder (MLS), Indian National Satellite System 3D (INSAT-3D), Indian National Satellite System 3D Repeat (INSAT-3DR), etc. In comparison with ground- and aircraft-based instruments, satellite instruments have the potential to expand their working vicinity [41]. Alongside synoptic scale satellite measurements, ground-based, balloon-borne, models, and aircraft measurements with certain temporal and spatial resolutions are also incorporated in order to ease the analysis of polar ozone science [42,43]. Moreover, reanalysis model data like Modern-Era Retrospective analysis for Research and Applications (MERRA), Modern-Era Retrospective analysis for Research and Applications-2 (MERRA-2), Global Modelling and Assimilation Office (GMAO), etc. can also provide ozone columnar measurements.

3. Life Cycle of Ozone

Stratospheric ozone is formed by photochemical reactions. It involves the interaction of solar radiation with different atmospheric gases specifically with oxygen. In 1930, Chapman put forward a theory of the formation of atomic oxygen which says the dissociation of O_2 in presence of UV photons is responsible for the formation of atomic oxygen (Equation (1)). And these highly reactive oxygen atoms react with oxygen molecules to form ozone molecules (Equation (2)).

$$O_2 + O_2 \rightarrow O + O \qquad \lambda \leq 242 \text{ nm} \tag{1}$$

$$O_2 + O + M \rightarrow O_3 + M \tag{2}$$

The M stands for any other molecule in the atmosphere most probably the abundant molecule like N_2 or O_2. And for the energy equilibrium of the reaction, this neutral body is needed. The dissociation of ozone molecule into O and O_2 is also undergone in the presence of UV photons (Equation (3)).

$$O_3 + h\nu \rightarrow O_2 + O \tag{3}$$

And the ozone is lost by reacting with free oxygen atoms (Equation (4)).

$$O_3 + O \rightarrow 2O_2 \tag{4}$$

The formation of ozone by solar UV photolysis is an endothermic reaction whereas the ozone dissociation reaction is an exothermic reaction. Since the presence of sunlight produces more ozone, Chapman's theory overestimates the tropics. With the help of meridional circulation, the transportation of tropically produced ozone to extra-tropics is taken place. This produced ozone gets destructed by particular highly reactive substances present over the stratosphere known as Ozone Depleting Substances (ODSs). These substances are majorly emitted at the surface of the Earth by various anthropogenic activities [1].

The catalytic destruction cycles balance the stratospheric chemical ozone production of the Chapman cycle. One of such cycles (Cycle-1) is shown below:

$$XO + O \rightarrow X + O_2$$
$$X + O_3 \rightarrow XO + O_2$$

Cycle-1: Net: $O + O_3 \rightarrow 2O_2$

X, the catalyst will get reproduced at the end of every cycle. A diatomic oxygen molecule is produced in the net reaction by the annihilation of one monoatomic oxygen and ozone molecule. In this way, thousands of ozone molecules get destructed and removed from the stratospheric layer. These catalyst gas molecules are produced by different anthropogenic actions occurring at the surface of Earth, and then these get reactive once reach stratosphere by some photochemical reactions [1].

There are certain common radical families which cause the depletion of ozone. HO_X family is one such family which involves atomic hydrogen H, hydroxyl radical OH, and the hydroperoxyl radical HO_2. Likewise, another radical nitric oxide (NO) also causes large ozone destruction. Furthermore, the reactive halogen gases

namely chlorine (Cl and ClO) and bromine (Br and BrO) also contribute to ozone destruction [1,44,45].

In wintertime across polar regions, the low-temperature circumstances at Polar Stratospheric Clouds (PSCs) assist in the large concentration of ClO. And it decreases the atomic oxygen concentrations there suppressing the occurrence of Cycle-1. Instead, the situation enhances two other cycles namely Cycle-2 and Cycle-3 which are shown below:

$$ClO + ClO + M \rightarrow (ClO)_2 + M$$
$$(ClO)_2 + h\nu \rightarrow ClOO + Cl$$
$$ClOO + M \rightarrow Cl + O_2 + M$$
$$2(Cl + O_3 \rightarrow ClO + O_2)$$

Cycle-2: Net: $O_3 + O_3 \rightarrow 3O_2$

$$ClO + BrO \rightarrow Cl + Br + O_2$$
$$Cl + O_3 \rightarrow BrO + O_2$$
$$Br + O_3 \rightarrow BrO + O_2$$

Cycle-3: Net: $O_3 + O_3 \rightarrow 3O_2$

Noticeably, Cycle-2 and Cycle-3 only occurred when there is enough ClO production come about. And more ClO abundance is detected in wintertime. Accordingly, Cycles 2 and 3 are responsible for the majority of Antarctic and Arctic ozone destruction. Also, the losses from these catalytic destruction cycles are controlled by temperature variations [46].

4. Role of Ozone Hole and Stratospheric Aerosols

It was noticed the declination within stratospheric ozone in the early 1970s across the extra-tropics [47]. All through the same decades, an investigation into the ozone trend in association with Supersonic Transport (SST) fleets and Chlorofluorocarbons (CFCs) was undertaken [48]. By the 1990s, the ozone destruction in both hemispheres got boosted up forward. Surprisingly, the Ozone Mass Deficiency (O_3MD) in the northern hemisphere exceeded the spring deficiencies of Antarctica in 1993 and 1995. Generally, winter-spring deficiencies are observed to be more than summer deficiencies [48]. And this ozone-depleted area is often referred to as an "Ozone Hole". This area became the minimum till date in 1994 with an ozone measurement of about 73 DU (Figure 4) (https://ozonewatch.gsfc.nasa.gov/).

This rapid spring stratospheric ozone decline over Antarctica caused the onset of different hypotheses in the 1980s. Then came forward two major hypotheses on unmeasured chemical reactions and on a dynamical concept consisting of a potential systematic variation in Antarctic circulation. Then this dynamical hypothesis got wide acceptance because of the intense correlation between lower stratospheric temperature and column ozone variations. Nonetheless, soon later this dynamic theory got rejected by the innovative integrated ground-based and aircraft measurements. And that observation led to the successful explanation of the significant correlation between chemical reactions happening at the lower stratosphere with the ozone depletion. Thus this chemical hypothesis prevails over the rejected dynamic hypothesis [49]. Consequently, both hemispheric ozone depletions are all noticed to be accompanied by a cold temperature of around 192 K and polar stratospheric cloud chemistry [49]. In recent past decades, during austral spring, it is comprehended that certain chemical reactions which involve chlorine, bromine, hydrogen, and nitrogen cause the depletion of ozone severely over the polar region [1,50]. Distinct maps of TCO exhibit the disparity and advancement in the ozone hole area during October

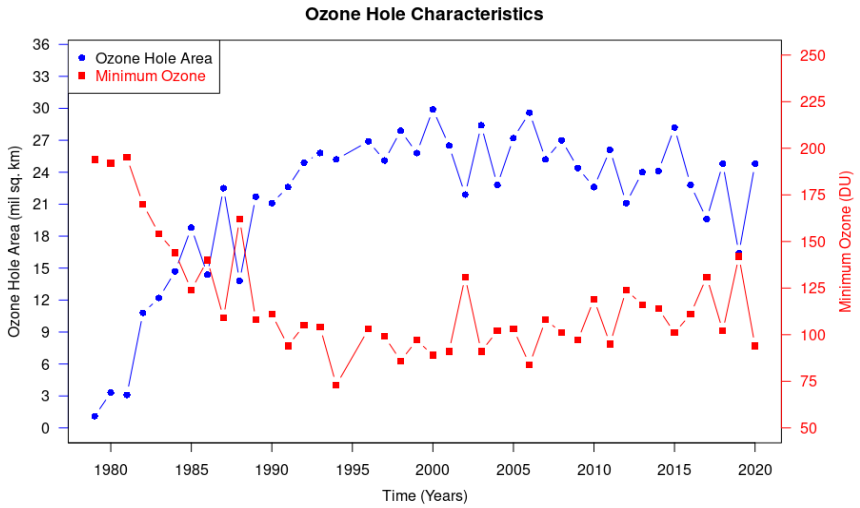

Figure 4. Southern hemispheric ozone hole area variation and minimum ozone features from 1979 up to 2020.

Source: https://ozonewatch.gsfc.nasa.gov/.

month for the period 1979 up to 2022 (Figure 5). The specific area is measured by representing a constant line of ozone of 220 DU (https://ozonewatch.gsfc.nasa.gov/). This particular value is selected because historic observations of pre-1979 have not shown a value of less than 220 DU. The 1979 evolving ozone hole characteristics continue till the end decade of the twentieth century. In the year 2002, it was observed that the particular Antarctic ozone hole is getting healed, but then again it resumed depletion but at a reduced pace. Similarly, in the year 2019, the ozone layer was expressing a recovery phase which further again went in vain by 2020 October.

In addition to that, recent direct Antarctic measurements have revealed the significant influence of bromine and chlorine compounds on columns with less than 220 DU ozone levels [51]. When the ozone level declines under 220 DU, it is investigated an upsurge in biologically vigorous UV radiation from 80 to 400% over the tropical, Arctic, and Antarctic regions [52]. The southern hemispheric climate change has been occurring in accordance with its ozone depletion throughout the recent past decades [53]. Around the previous 40 years, a poleward shift of extratropical circulation happened due to ozone depletion along the polar region. Subsequently, the subtropical precipitation and thereby hydrological cycle over the region has also become substantially disturbed [54]. In spring, the inert halide salts across the polar boundary layer got converted into highly reactive halogen species which deplete the ozone around the region up to an extent of nearly zero level [55].

A new parameter termed Equivalent Effective Stratospheric Chlorine (EESC) got introduced so as to particularize the ease of ozone variability investigation. A temporal examination of this EESC together with the Freon-11 (CFC-11) is conducted and got to find a strong

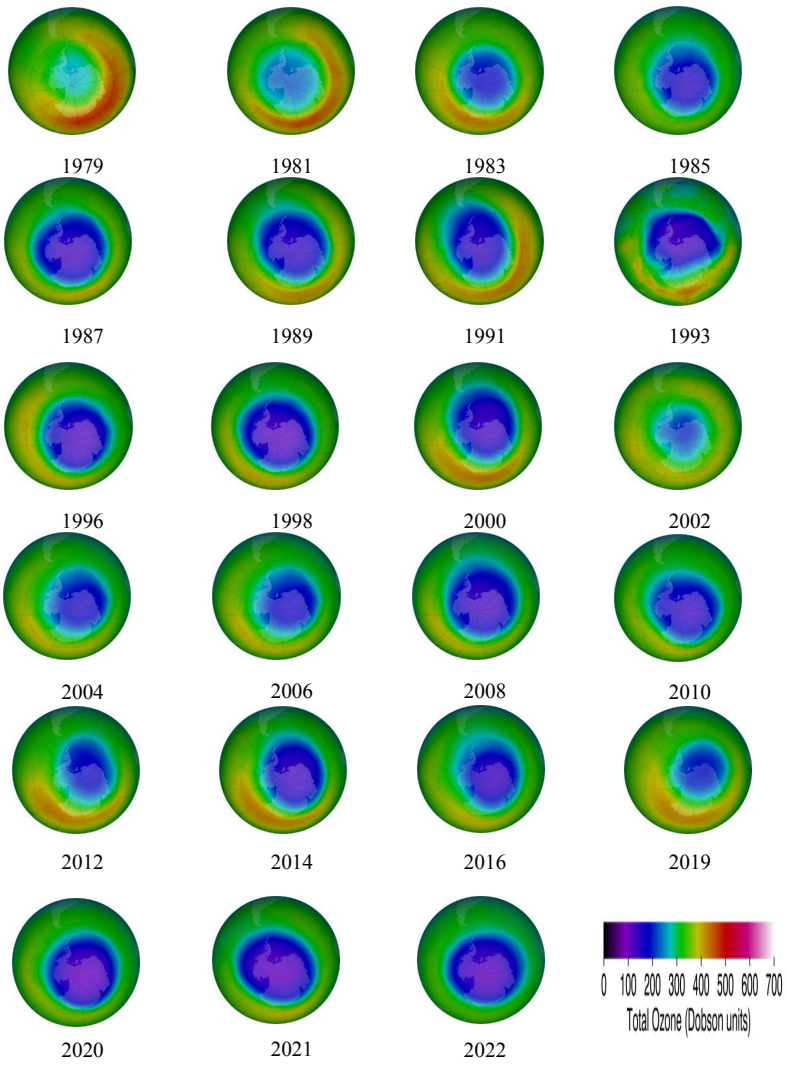

Figure 5. Antarctic ozone hole monthly mean characteristics for October from 1979 up to 2022 (with intermediate year intervals; https://ozonewatch.gsfc.nasa.gov/).

peak during the late 1990s and early 2000s (Figure 6) [56]. And the corresponding ozone levels experienced a considerable decline. A strong recovering tendency of the ozone hole is also observed from the projected analysis [56].

Since the 1980s, the Antarctic ozone layer has been experiencing a significant decline in the ozone mixing ratio of 0.01 to 0.1 ppm during spring seasons. And this corresponds to a regional chemical loss of around 95% to 99%. On the contrary, the north-polar stratospheric ozone loss has been considerably better than that of the south with a maximum value of only 0.5 ppm. Nevertheless, in spring 2020 a huge ozone loss happened over the Arctic at an altitude of around 18 km. The Ozonesondes observations reveal a local chemical loss of about 93%. A strong and long lasted cold polar vortex was observed to be the major cause of this unforeseen Arctic chemical loss [57].

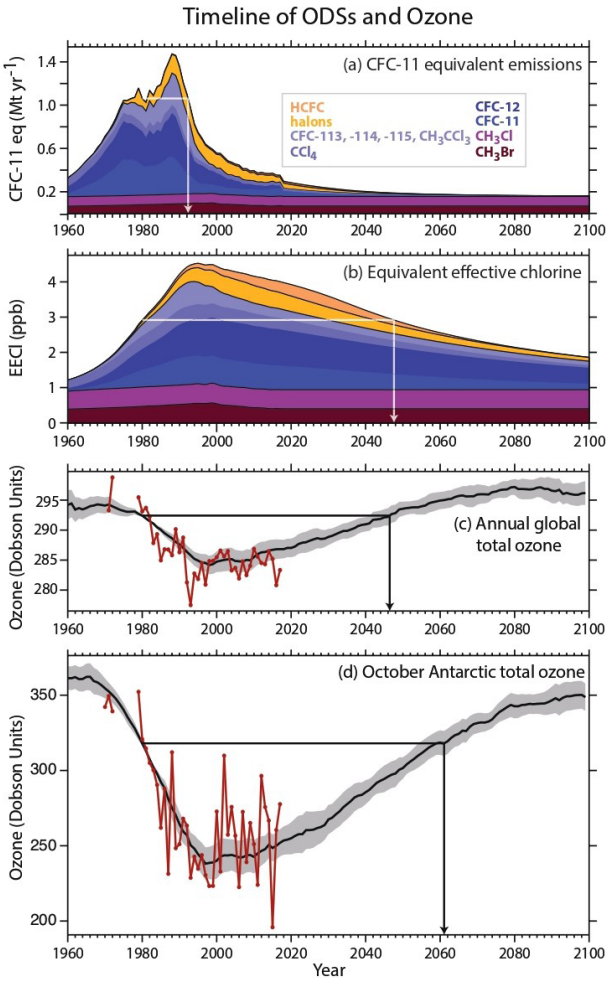

Figure 6. Characteristic temporal variation of Ozone and Ozone Depleting Substances (ODSs). An ozone hole restorative condition is witnessed after a profound decline during the late 1990s and early 2000s [56].

The progress of recent three-dimensional stratospheric ozone models has helped extensively in predicting reliable ozone level fluctuations in comparison with the one-dimensional models of the 1970s. Flawless computational model development and refined prediction obviously come from impeccable observation data [58]. These are majorly produced by volcanic eruptions, and infrequently by aerosols formed from other natural and anthropogenic actions [59]. Highly vigorous volcanic eruptions in the tropics cause the ejection and transport of large quantities of gases like sulphate, hydrogen halides, etc. into the stratosphere from where they spread globally by the action of large-scale meridional circulations [52,60]. The 1991 Mount Pinatubo volcanic eruption incident caused an explosive injection of sulphate aerosols into the stratosphere. It was observed that this event had resulted in polar region ozone depletion in the following few years. Though it caused the ozone layer destruction, the "Earth cooling effect" contributed by those sulphate aerosol ejections was praised and suggested as a remedial tool to defend against global warming. On the other hand, the assessment of the required quantity of sulphates in order to compensate with the amount for surface warming CO_2 and its ozone-depleting action made that trial impossible [61]. Similarly, another study on aerosols of polar regions revealed that the Solar Proton Events (SPEs) caused short-term ozone depletion events by the production of nitrate aerosols would also result in significant impacts on our biosphere [62]. The aerosol optical depth (AOD) spectral variations triggered by anthropogenic actions are found to be playing a key role in ozone variations and Earth-Atmosphere radiation balances over the Arctic which in turn will affect the regional and global climate change [63].

Many human activities are observed transcending natural processes and causing precarious aftermaths in the environment. Production of high-risk chemical compounds like CFCs is also observed to be contributing to certain dangerous events such as ozone layer depletion. Furthermore, these human activities have currently levelled up to consider profound geological forces. The activities like fossil fuel burning, land-use changes, and deforestation are some examples. Therefore, an assignment of a new term "Anthropocene" has come into the limelight compulsorily in order to represent the current geological epoch. And it is considered that the epoch started in the year 1784 when the designing of James Watt's steam engine has got taken place [64].

5. Polar Vortex and Polar Stratospheric Clouds

The area in the atmosphere at which the rotational motion of fluid occurs with respect to a particular axis is

called an atmospheric vortex. And the Polar Vortex is one such vortex observed over polar regions where an eastward movement of fluid (gaseous atmosphere) takes place. The northern hemispheric polar vortex will be centred at the Arctic and the southern hemisphere will have a vortex with a rotation axis around Antarctica [65].

1) ***Arctic Polar Vortex:*** In the northern hemisphere, the Arctic air being the coldest in comparison with its southward air circulation will undergo a cold temperate vortex flowing from west to east. And as the zone of the interface of cold Arctic air with warm subtropical air, there at the margin of intersection witnesses the polar front jet stream [66]. In the year 2019-2020, the winter-spring seasons experienced a remarkably low temperature and an established boreal polar vortex which led to widespread ozone depletion in the Arctic region [57]. And these ozone depletions are only localized over polar vortex regions [67].

2) ***Antarctic Polar Vortex:*** Analogous to the Arctic vortex system, in the southern hemisphere, a cold vortex formation establishes which interface with southern hemispheric mid-latitude air where causing the formation of the austral polar frontal jet stream [66]. In general, these polar vortices comprise a large low-pressure area that circulates in an anti-clockwise direction in the northern hemisphere and in a clockwise direction southern hemisphere. More importantly, it is an eastward rotation of atmospheric fluid in both hemispheres. The vortex shape can vary from a circle to some irregular meanders extending up to the equator [65].

Polar Stratospheric Clouds (PSC) are clouds present at an elevation range of 15 km up to 25 km. They are well witnessed during winter time over polar regions at twilight. It is found that these high-altitude clouds cause ozone depletion in the stratosphere. These PSCs are formed at very lower temperatures. PSCs are associated with ozone destruction mainly in two ways; PSCs provide a surface for the establishment of reactive ozone-depleting chlorine, and these PSCs will take part in the removal of nitrogen compounds that regulate the destructive nature of chlorine [59,68]. In the 2019-2020 winter, a massive loss of Arctic stratospheric ozone occurred. Other analogous exceptional Arctic stratospheric ozone depletions happened in 2015-2016, 2010-2011, and 1996-1997 winter times. All these events owe to the lowest polar vortex temperatures which made it easy for the formation of PSCs. This resulted in the denitrification and dehydration of the Arctic polar vortex that further caused the enhancement of ozone depletion [69].

6. Ozone and Climate Change

There exists a convincing association between stratospheric ozone chemistry and annular modes [70]. An annular mode is a significant pattern of climatic variability observed over northern and southern hemispheres. Northern Annular Mode (NAM) is intense during boreal winter and Southern Annular Mode (SAM) is larger during austral summer. Both the annular modes play a strategic responsibility in climate change [71].

The significant causes of the impact of ozone layer depletion on climate change are due to solar radiation absorption characteristics of ozone, its GHG features, and alteration of tropopause height [72]. In order to retrieve a better quantification of UV radiation, since the 1990s several stations have been operating for the continuous measurement of radiation. The UV radiation quantification depends on factors namely latitude, longitude, height, incident angle, azimuth angle, wavelength, and polarisation [73]. For the sake of reversal of climate change effects, the Paris Accord-2016 has put forward certain suggestions to phase out the usage of hazardous synthetic refrigerants. Currently, the GHGs used in refrigeration, air-conditioning, and heat-pumping systems are regulated under Kyoto protocol-1997 [74]. By choosing natural refrigerants, further intensification in GHGs can be regulated [74].

In 1992, so as to provide a comprehensive scientific base and plan for World Meteorological Organization (WMO)—UNEP ozone assessments, a project named Stratospheric Processes And Role in Climate (SPARC) was implemented by World Climate Research Programme (WCRP) [75]. There originated three ozone assessment panels of experts under UNEP namely the Environmental Effects Assessment Panel (EEAP), Scientific Assessment Panel (SAP), and Technology and Economic Assessment Panel (TEAP). The EEAP works on the impacts of UV rays on human health, global climate change, terrestrial and aquatic ecosystems, and on air quality attributes [76].

By the comparison of UV measurements with model simulations, UV-B radiation is found to be decreasing at the Earth's surface. Therefore, the Montreal Protocol is observed to be showing its efficacy. On the contrary, though the ozone layer over Antarctica is getting recovered, the corresponding reduction in UV-B radiation has not been witnessed [77]. During the summer season, it is perceived that the Antarctic ozone depletion strongly controls climate change in the southern hemisphere [78]. Also, in another analysis, it has been shown that the Arctic ozone inter-annual variability makes modifications in the climate of northern hemispheric mid-latitudes. In the course

of positive Arctic ozone anomaly events, it is found that it strengthens the precipitation over central China. And during its negative phase, the precipitation along the same region is suppressed [79]. The concept of potentials namely Ozone Depletion Potential (ODP) and Global Warming Potential (GWP) has been widely used in policymaking by integrating them with ozone and climate issues [80]. A comparative study between the emissions, radiative forcing, and surface temperature by integrating all these with variations of ODSs, high GWP HFCs, and low GWP HFCs has been conducted (Figure 7). Throughout the observations, a co-existing feature of high GWP HFC is noticed along with ODS to a considerable extent [56].

The cases of UV radiation-caused cutaneous malignant melanoma are showing an increasing trend in northern European countries. Even though, Australia and New Zealand are the leading countries in terms of melanoma affected. The same countries are showing a good recovery rate as well [81].

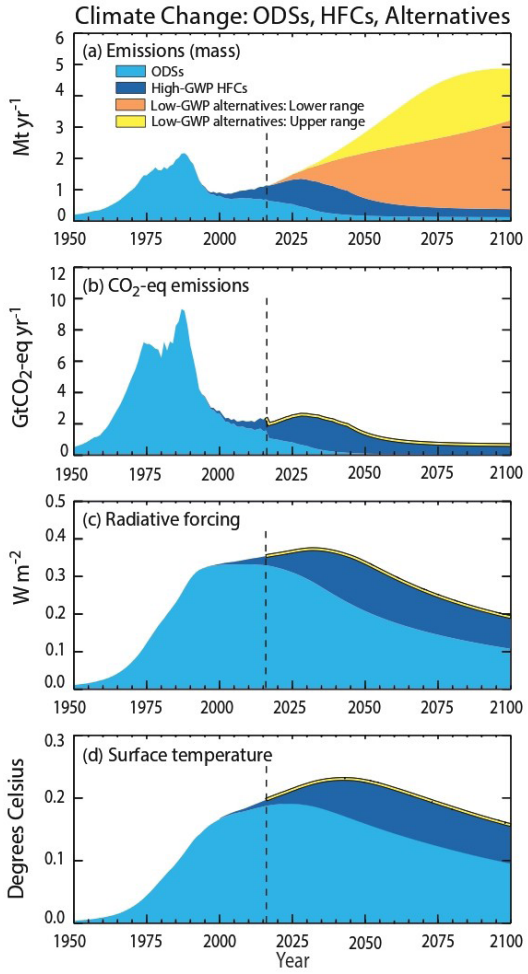

Figure 7. Temporal variation of different Ozone Depleting Substances (ODSs) and their co-existence with emissions, radiative forcing, and surface temperature [56].

7. Consequences of Ozone Layer Depletion

- As ozone is an effective absorber of UV radiation, its depletion will cause a substantial increase in ground-level abundance of UV radiation [82].
- The decline in stratospheric ozone will cause an upsurge in extratropical tropospheric ozone level [80]. When the precursor molecules such as NOX, and VOCs react with sunlight, surface ozone is produced. And this is a key air pollutant. And these precursor molecules can be formed by biomass burning, etc. [83]. Such processes are enhanced by the tropospheric oxidizer OH [84].
- Increased production of Vitamin D because of the extensive solar UV radiation availability over the Earth's surface [85].
- Cataract is the major reason for blindness in the world. And it is frightening that a 1% decrease in the ozone layer would cause a 0.3% to 0.6% increased chance of cataracts [86,87]. Because of the oxidative agents like oxygen produced by UV radiation, the cornea and lens of the eye would get damaged. In addition to cortical cataracts, photokeratitis, pterygium, and macular degeneration can also be caused [88].
- Overexposing to UV due to the depletion of the ozone layer would cause sunburns and skin cancers. There are mainly two categories of skin cancers. One is melanoma cancer and the second one is non-melanoma. The former is more detrimental than the latter. In non-melanoma, there includes basal cell carcinoma and squamous cell carcinoma [89].
- The fatal UV-B radiations can damage DNA. It can harm biomolecules like lipids, proteins, and nucleic acids. It can even enhance mutations in DNA [90].
- As a consequence of ozone layer depletion, reduced oxygen production got enhanced in the Earth's atmosphere which further initiate the formation of hydrogen peroxide (H_2O_2). This produced hydrogen peroxide is toxic and a water pollutant. Thus it adversely affects human health [91].
- UV radiation exposure would also result in some deadly lungs related health issues like Emphysema, Asthma, and Bronchitis [90].
- Furthermore, the ozone layer depletion affects other terrestrial and aquatic ecosystems very dangerously and it would alter various biogeochemical cycles [91].
- Due to the stratospheric ozone destruction, the mean age of Antarctic summer air in the lower stratosphere has become increased. This is mainly because of intense Antarctic downwelling that fetches older

air from the upper to lower stratosphere. Also, a seasonal obstruction in austral polar vortex breakup stops new mid-latitude air from mixing up with the internal old air of the vortex [92].

8. International Commitments

The necessary monitoring of the deterioration of the ozone layer has been of primary importance since the beginning of the 1980s [93]. From the early 1980s, there have been several international ozone assessments that paved the foundation for the Vienna convention and Montreal protocol [23].

Vienna Convention—1985: By the initiative of the United Nations Environment Programme (UNEP), the conciliation of the Vienna convention began in January 1982. And all these initiatives were taking place under the leadership of a UNEP council formed in May 1981 to protect the ozone layer [94]. The Vienna convention was just a preamble and legal foundation for the Montreal protocol. It does not depend on some particular chemical compound's legitimate regulation at a global level. The Vienna ozone convention was one of the first international agreements on environmental protection [94].

Montreal Protocol—1987: It is an international treaty signed on 26th August 1987 to reduce the production and emission of ODSs. But it came into effect on 26th August 1989. Since then many amendments and adjustments to this protocol have entered into force. Around nine revisions have come into operation till 2018 (Table 1). Many modifications have been implemented to the Montreal protocol to date [95]. In the 1992 revisions, CFCs have got substituted by relatively less depleting Hydrochlorofluorocarbons (HCFCs) [96]. Later on, HCFCs have also got replaced by Hydrofluorocarbons (HFCs) as those were noticed to be having an ozone-depleting potential of nearly zero. Although, HFCs have got turned up to be causing global warming as per the 1997 Kyoto protocol assessments [95]. Kigali amendment on 15th October 2016 came into a decision to phase down HFCs under the Montreal protocol. Then attended 197 countries came into an agreement to cut down the manufacturing and consumption of HFCs by greater than 80% by the next 30 years. To date, we can consider this Montreal Protocol a success and it is one of the greatest successful multilateral environmental agreements in history. United States National Oceanic and Atmospheric Administration (NOAA) observed that the concentration of various ODSs has fallen below 1980 levels after an increase in the early 2000s. They also predicted that the concentration of

Table 1. International commitments on ozone layer depletion [56].

Year	Policy Decisions	Scientific Reports
1981		The Stratosphere 1981: Theory and Measurements. WMO No. 11.
1985	Vienna Convention	Atmospheric Ozone 1985. Three volumes. WMO No. 16
1987	Montreal Protocol	
1988		International Ozone Trends Panel Report 1988. Two volumes. WMO No. 18.
1989		Scientific Assessment of Stratospheric Ozone: 1989. Two volumes. WMO No. 20
1990	London Adjustment and Amendment	
1991		Scientific Assessment of Ozone Depletion: 1991. WMO No. 25.
1992		Methyl Bromide: Its Atmospheric Science, Technology, and Economics (Montreal Protocol Assessment Supplement). UNEP (1992)
1992	Copenhagen Adjustment and Amendment	
1994		Scientific Assessment of Ozone Depletion: 1994. WMO No. 37.
1995	Vienna Adjustment	
1997	Montreal Adjustment and Amendment	
1998		Scientific Assessment of Ozone Depletion: 1998. WMO No. 44.
1999	Beijing Adjustment and Amendment	
2002		Scientific Assessment of Ozone Depletion: 2002. WMO No. 47.
2006		Scientific Assessment of Ozone Depletion: 2006. WMO No. 50.
2007	Montreal Adjustment	
2010		Scientific Assessment of Ozone Depletion: 2010. WMO No. 52.
2014		Scientific Assessment of Ozone Depletion: 2014. WMO No. 55.
2016	Kigali Amendment	
2018		Scientific Assessment of Ozone Depletion: 2018. WMO No. 58.

CFCs would also decrease below 1980 levels by 2050 [95]. Furthermore, ODS manufacturing sank from 1.2 million tons in 1986 to 23000 tons in 2016. By the same token, its consumption also has got plunged to 22000 tons in 2016 from 86000 tons in 1986 [76]. The UNEP Ozone Secretariat investigated that the global usage of CFC would have been more than 3 million tons in 2010 and would have become 8 million tons by 2060. if it happens to result in the depletion of half of the ozone layer by 2035. In 2018, a study revealed that the cut down of chlorine from ODSs caused healing of ozone hole [97,98].

9. Conclusions

At surface and tropospheric levels warming is instigated by the ozone hole formation whereas at the stratosphere it provides a cooling effect [99]. Being the major side-effect of ozone layer depletion, increased UV-B on the surface of Earth caused substantial health issues for humans and other living beings. Over the Arctic, the earlier chlorine activation and the depletion occurred by 2010 and 2019 Novembers respectively for 2011 and 2020. In addition, it longed till the end of spring. These events are attributed to the weak polar vortices of corresponding seasons. Contrary to ozone destruction, the primary impact of ODS on the Arctic is observed to be affected by the effect of radiative warming [100].

All the international treaties for the protection of the ozone layer have their own participation in restraining the production of ODSs. Nearly all ODSs fall under the category of GHGs. Therefore they too broadly contribute to global warming [101]. Remarkably the Montreal protocol has been a great success so far, the inorganic chlorine level was noticed to be decreasing and the ozone hole reinvigoration was found to be happening over the Antarctic stratosphere. The long lifespan of the precursor molecules delays the expected speedy recovery of the ozone layer up to the rest of the twenty-first century. However, by the mid-century, the mid-latitude ozone will come back to the 1980s level. In addition to that, the UV-B irradiance at mid-latitudes is also getting declined even though it has some attributions with aerosols and clouds. Nonetheless, polar latitudes show a substantial increase in the same. Overall, specific uncertainties exist with respect to the rate of recovery of the ozone layer. Unexpected hike in the emission of natural ODSs namely CH_3Cl and CH_3Br along with the climate change-induced stratospheric structural-changes which further will obstruct the ozone depletion recovery [102]. The world without a Montreal protocol would have been having tripled UV radiation of current time by 2065 across the mid-latitudes [8]. A robust interaction between GHG-induced climate change and ozone destruction scenarios has been contemplated throughout recent past decades. Self-awareness in reducing ODS partly benefited in decreasing GHG emissions globally. The projected decline in radiative forcing with respect to CFC cut-down has been underestimated. Although ozone shows tendencies for recovery, the future evolution of UV-B radiation will be determined by the ongoing climate change and the decreasing ODSs. Recent studies show cloud cover generally decreases, leading to increased solar radiation, apart from the high latitudes, where no significant changes are observed. Total ozone shows an increasing trend due to the reduction in ODSs, while a decrease is observed after 2050 on a near-global scale due to the increasing GHGs. UV trends are a combination of changes in ozone and cloud cover, while at high latitudes, the decreasing surface albedo in the second half of the 21st century has a significant influence on the surface UV radiation.

Rather than the frequent variants in the usage of synthetic refrigerants, natural refrigerants are the long-term alternatives [103]. The present-day anticipated annual global total ozone recovery to 1980s levels is approximated to the mid-2040s. The Antarctic ozone layer restoring noticed to be happening every September [104]. The climate change—ozone depletion association would be a challenging task for the scientific world to project the future ozone scenario flawlessly. Persistent high quality ground-based and satellite ozone measurements only will assure the errorless projections [69].

Authors' Contribution

M. M. Karadan: Conceptualization of the study, data archiving and preparation of the initial draft of the manuscript; **P.V.S. Raju**: Interpretation of the concept and finalization of the manuscript; **P.C.S. Devara**: Guidance and help in finalization of manuscript.

Acknowledgement

The authors express their sincere gratitude to all Authorities of AUR, Jaipur and AUH, Gurugram. Thanks, are also due to the anonymous reviewer for critical comments and valuable suggestions, which improved the scientific content of the manuscript.

Conflicts of Interest

No potential conflict of interest was reported by the author(s).

References

[1] Langematz, U., 2019. Stratospheric ozone: Down

and up through the anthropocene. ChemTexts. 5(8). DOI: https://doi.org/10.1007/s40828-019-0082-7

[2] Mani, A., Sreedharan, C.R., 1973. Studies of variations in the vertical ozone profiles over India. Pure and Applied Geophysics. 106, 1180-1191. DOI: https://doi.org/10.1007/BF00881070

[3] Sreedharan, C.R., Mani, A., 1973. Ozone and temperature changes in the lower stratosphere. Pure and Applied Geophysics. 106, 1576-1580. DOI: https://doi.org/10.1007/BF00881106

[4] Mani, A., Sreedharan, C.R., Joseph, P.V., et al., 1973. Studies of the vertical distribution of atmospheric ozone in association with western disturbances over India. Pure and Applied Geophysics. 106, 1192-1199. DOI: https://doi.org/10.1007/BF00881071

[5] World Meteorological Organization, 2006. World Meteorological Organization Global Ozone Research and Monitoring Project-Report No. 50 National Oceanic and Atmospheric Administration National Aeronautics and Space Administration United Nations Environment Programme World Meteorological Organization European Commission. Available from: https://library.wmo.int/index.php?lvl=notice_display&id=6414#.ZAcvy3ZBxPY

[6] Wang, W.Ch., Tanaka, H., 2009. Tropospheric ozone climate-chemistry interaction: Aspects of climate changes. Twenty Years of Ozone Decline. Springer: Dordrecht. pp. 291-295.

[7] Chipperfield, M.P., 2018. On the cause of recent variations in lower stratospheric ozone. Geophysical Research Letters. 45, 5718-5726. DOI: https://doi.org/10.1029/2018GL078071

[8] McKenzie, R.L., 2011. Ozone depletion and climate change: Impacts on UV radiation. Photochemical and Photobiological Sciences. 10, 182-198. DOI: https://doi.org/10.1039/c0pp90034f

[9] Vingarzan, R., 2004. A review of surface ozone background levels and trends. Atmospheric Environment. 38, 3431-3442. DOI: https://doi.org/10.1016/j.atmosenv.2004.03.030

[10] Manney, G.L., 2020. Record-low arctic stratospheric ozone in 2020: MLS observations of chemical processes and comparisons with previous extreme winters. Geophysical Research Letters. 47(16). DOI: https://doi.org/10.1029/2020GL089063

[11] Díaz, J., Ortiz, C., Falcón, I., et al., 2018. Short-term effect of tropospheric ozone on daily mortality in Spain. Atmospheric Environment. 187, 107-116. DOI: https://doi.org/10.1016/j.atmosenv.2018.05.059

[12] Monks, P.S., 2015. Tropospheric ozone and its precursors from the urban to the global scale from air quality to short-lived climate forcer. Atmospheric Chemistry and Physics. 15, 8889-8973. DOI: https://doi.org/10.5194/acp-15-8889-2015

[13] Gao, Y., Fu, J.S., Drake, J.B., et al., 2013. The impact of emission and climate change on ozone in the United States under representative concentration pathways (RCPs). Atmospheric Chemistry and Physics. 13, 9607-9621. DOI: https://doi.org/10.5194/acp-13-9607-2013

[14] Mills, G., 2018. Tropospheric ozone assessment report: Present-day tropospheric ozone distribution and trends relevant to vegetation. Elementa. 6(47). DOI: https://doi.org/10.1525/elementa.302

[15] Cooper, O.R., 2014. Global distribution and trends of tropospheric ozone: An observation-based review. Elementa. 2, 000029. DOI: https://doi.org/10.12952/journal.elementa.000029

[16] Granier, C., 2011. Evolution of anthropogenic and biomass burning emissions of air pollutants at global and regional scales during the 1980-2010 period. Climate Change. 109, 163-190. DOI: https://doi.org/10.1007/s10584-011-0154-1

[17] Zhang, Y., 2016. Tropospheric ozone change from 1980 to 2010 dominated by equatorward redistribution of emissions. Nature Geoscience. 9, 875-879. DOI: https://doi.org/10.1038/ngeo2827

[18] Mills, G., Wagg, S., Harmens, H., 2013. Ozone pollution: Impacts on ecosystem services and biodiversity. ICP Vegetation Programme Coordination Centre: UK. http://icpvegetation.ceh.ac.uk

[19] Ainsworth, E.A., Yendrek, C.R., Sitch, S., et al., 2012. The effects of tropospheric ozone on net primary productivity and implications for climate change. Annual Review of Plant Biology. 63, 637-661. DOI: https://doi.org/10.1146/annurev-arplant-042110-103829

[20] Mills, G., Harmens, H., 2011. Ozone pollution: Report Prepared by the Icp Vegetation Ozone Pollution: A Hidden Threat to Food Security [Internet]. Available from: http://icpvegetation.ceh.ac.uk

[21] Sun, G., 2012. Interactive influences of ozone and climate on streamflow of forested watersheds. Global Change Biology. 18, 3395-3409. DOI: https://doi.org/10.1111/j.1365-2486.2012.02787.x

[22] Fumagalli, I., Gimeno, B.S., Velissariou, D., et al., 2001. Evidence of ozone-induced adverse effects on crops in the Mediterranean region. Atmospheric Environment. 35(14), 2583-2587.

DOI: https://doi.org/10.1016/j.envpol.2008.09.001

[23] Bojkov Rumen, D., Balis, D.S., 2009. The history of total ozone measurements: The early search for signs of a trend and an update. Twenty years of ozone decline. Springer: Dordrecht. pp. 73-110.

[24] Sreedharan, C.U., 1968. An Indian electrochemical ozonesonde. Journal of Scientific Instruments. 1(10), 995-997.
DOI: http://dx.doi.org/10.1007/978-90-481-2469-5_7

[25] Kerr, J.B., 1994. The 1991 WMO international ozonesonde intercomparison at Vanscoy, Canada. Atmosphere Ocean. 32, 685-716.
DOI: https://doi.org/10.1080/07055900.1994.9649518

[26] Hofmann, D.J., 2009. International balloon measurements for ozone research. Twenty Years of Ozone Decline. Springer, Dordrecht. pp. 157-172.
DOI: https://doi.org/10.1007/978-90-481-2469-5_11

[27] Wazir, M., 2011. Estimation of regional stratospheric ozone concerning Pakistan. Pakistan Journal of Meteorology. 7, 14.

[28] Köhler, U., 2017. Optical characterization of three reference Dobsons in the ATMOZ project - Verification of G. M. B. Dobson's original specifications. Atmospheric Measurement Techniques. 11, 1989-1999.
DOI: https://doi.org/10.5194/amt-11-1989-2018

[29] Nichol, S.E., 2018. Past, present and future. Weather Climate and Society. 38, 16-27.

[30] Komhyr, W.D., Mateer, C.L., Hudson, R.D., 1993. Effective Bass-Paur 1985 ozone absorption coefficients for use with Dobson ozone spectrophotometers. Journal of Geophysical Research: Atmospheres. 98, 20451-20465.
DOI: https://doi.org/10.1029/93JD00602

[31] Bass, A.M., Paur, R.J., 1985. The ultraviolet cross-sections of ozone: I. the measurements. Atmospheric Ozone. Springer, Dordrecht. pp. 606-610.
DOI: https://doi.org/10.1007/978-94-009-5313-0_120

[32] Basher, R.E., 1985. Review of the Dobson Spectrophotometer and its accuracy. Atmospheric ozone. Springer: Dordrecht. pp. 387-391.
DOI: https://doi.org/10.1007/978-94-009-5313-0_78

[33] Hendrick, F., 2011. NDACC/SAOZ UV-visible total ozone measurements: Improved retrieval and comparison with correlative ground-based and satellite observations. Atmospheric Chemistry and Physics. 11, 5975-5995.
DOI: https://doi.org/10.5194/acp-11-5975-2011

[34] Govindan, S.S., Ariffin, M., Yik, D.J., et al., 2011. Characteristics and variability of total ozone concentration over Petaling Jaya, Malaysia using the brewer ozone spectrophotometer. World Climate Research Program—Open Science. 11(7), 746.

[35] Scarnato, B., Staehelin, J., Stübi, R., et al., 2010. Long-term total ozone observations at Arosa (Switzerland) with Dobson and Brewer instruments (1988-2007). Journal of Geophysical Research Atmospheres. 115(D13).
DOI: https://doi.org/10.1029/2009JD011908

[36] Pommereau, J.P., Goutaft, F., 1988. O_3 and NO_2 ground-based measurements by visible spectrometry during Arctic winter and spring. Geophysical Research Letters. 15(8), 891-894.
DOI: https://doi.org/10.1029/GL015i008p00891

[37] Kuttippurath, J., 2013. Antarctic ozone loss in 1979-2010: First sign of ozone recovery. Atmospheric Chemistry and Physics. 13, 1625-1635.
DOI: https://doi.org/10.5194/acp-13-1625-2013

[38] Kuttippurath, J., Kumar, P., Nair, P.J., et al., 2018. Accuracy of satellite total column ozone measurements in polar vortex conditions: Comparison with ground-based observations in 1979-2013. Remote Sensing Environment. 209, 648-659.
DOI: https://doi.org/10.1016/j.rse.2018.02.054

[39] Hendrick, F., 2011. NDACC/SAOZ UV-visible total ozone measurements: Improved retrieval and comparison with correlative ground-based and satellite observations. Atmospheric Chemistry and Physics. 11, 5975-5995.
DOI: https://doi.org/10.5194/acp-11-5975-2011

[40] Richter, A., Burrows, J., Nüss, H., et al., 2005. Increase in tropospheric nitrogen dioxide over China observed from space. Nature. 437, 129-132.
DOI: https://doi.org/10.1038/nature04092

[41] Bhartia, P.K., 2009. Role of satellite measurements in the discovery of stratospheric ozone depletion. Twenty Years of Ozone Decline. Springer: Dordrecht. pp. 183-189.
DOI: https://doi.org/10.1007/978-90-481-2469-5_13

[42] Kurylo, M.J., 2009. The role of airborne science in the study of polar ozone. Twenty years of ozone decline. Springer: Dordrecht. pp. 173-182.
DOI: https://doi.org/10.1007/978-90-481-2469-5_12

[43] Thompson, A.M., 2009. An overview of strategic ozone sounding networks: Insights into ozone Budgets, UT/LS processes and tropical climate signatures. Twenty Years of Ozone Decline. p. 237-249.
DOI: https://doi.org/10.1007/978-90-481-2469-5_17

[44] Bates, D.R., Nicolet, M., 1950. The photochemistry of atmospheric water vapor. Journal of Geophysical Research. 55, 301-327.

DOI: https://doi.org/10.1029/JZ055i003p00301

[45] Subbaraya, B.H., 1994. Variability in the vertical distribution of ozone measured over Thumba during the 1990 DYANA campaign. Journal of Armospheric and Terresrnol Physics. 56(13-14), 1915-1922. DOI: https://ui.adsabs.harvard.edu/link_gateway/1994JATP...56.1915S/doi:10.1016/0021-9169(94)90018-3

[46] Newman, P.A., Nash, E.R., Douglass, A.R., et al., 2007. Estimating when the Antarctic ozone hole will recover. Twenty years of ozone decline. Springer: Dordrecht. pp. 191-200. DOI: https://doi.org/10.1007/978-90-481-2469-5_14

[47] Harris, N.R.P., 2009. The long history of ozone: Analyses of recent measurements. Twenty years of ozone decline. Springer: Dordrecht. pp. 111-117. DOI: https://doi.org/10.1007/978-90-481-2469-5_8

[48] Schoeberl Mark, R., Rodriguez, J.M., 2009. The rise and fall of dynamical theories of the ozone hole. Twenty Years of Ozone Decline. Springer: Dordrecht. pp. 263-272. DOI: https://doi.org/10.1007/978-90-481-2469-5_19

[49] Solomon, S., Kinnison, D., Bandoro, J., et al., 2015. Simulation of polar ozone depletion: An update. Journal of Geophysical Research. 120, 7958-7974. DOI: https://doi.org/10.1002/2015JD023365

[50] Wang, S., 2019. Direct detection of atmospheric atomic bromine leading to mercury and ozone depletion. Earth Atmospheric and Planetary Sciences. 116(29), 14479-14484. DOI: https://doi.org/10.1073/pnas.1900613116

[51] Bodeker, G.E., Shiona, H., Eskes, H., 2005. Indicators of antarctic ozone depletion. Atmospheric Chemistry and Physics. 5, 2603-2615. DOI: https://doi.org/10.5194/acp-5-2603-2005

[52] Brenna, H., Kutterolf, S., Krüger, K., 2019. Global ozone depletion and increase of UV radiation caused by pre-industrial tropical volcanic eruptions. Scientific Reports. 9, 9435. DOI: https://doi.org/10.1038/s41598-019-45630-0

[53] Previdi, M., Polvani, L.M., 2014. Climate system response to stratospheric ozone depletion and recovery. Quraterly Journal of Royal Meteorol Society. 140, 2401-2419. DOI: https://doi.org/10.1002/qj.2330

[54] Kang, S.M., Polvani, L.M., Fyfe, J.C., et al., 2011. Impact of polar ozone depletion on subtropical precipitation. Science. 332, 951. DOI: https://doi.org/10.1126/science.1202131

[55] Simpson, W.R., Von Glasow, R., Riedel, K., et al., 2007. Halogens and their role in polar boundary-layer ozone depletion. Atmospheric Chemistry and Physics. 7(16), 4375-4418. DOI: https://doi.org/10.5194/acp-7-4375-2007

[56] World Meteorological Organization United States, 2018. National Oceanic and Atmospheric Administration, United States. National Aeronautics and Space Administration, United Nations Environment Programme & European Commission. Scientific assessment of ozone depletion. Available from: https://library.wmo.int/index.php?lvl=notice_display&id=20763#.ZAcwNXZBxPY

[57] Wohltmann, I., 2020. Near-complete local reduction of arctic stratospheric ozone by severe chemical loss in spring 2020. Geophysical Research Letters. 47(20), e2020GL089547. DOI: https://doi.org/10.1029/2020GL089547

[58] Douglass, A.R., 2009. Global observations—The key to model development and improved assessments. Twenty Years of Ozone Decline. Springer: Berlin. pp. 251-259. DOI: https://doi.org/10.1007/978-90-481-2469-5_18

[59] Zhu, Y., 2018. Stratospheric aerosols, polar stratospheric clouds, and polar ozone depletion after the mount calbuco eruption in 2015. Journal of Geophysical Research Atmosheres. 123, 12. DOI: https://doi.org/10.1029/2018JD028974

[60] Eric Klobas, J., Wilmouth, D.M., Weisenstein, D.K., et al., 2017. Ozone depletion following future volcanic eruptions. Geophysical Research Letters. 44(14), 7490-7499. DOI: https://doi.org/10.1002/2017GL073972

[61] Tilmes, S., Müller, R., Salawitch, R., 2008. The sensitivity of polar ozone depletion to proposed geoengineering schemes. Science. 320, 1201. DOI: https://doi.org/10.1126/science.1153966

[62] Sonabawne, S.M., Devara, P.C.S., Rahul, P.R.C., et al., 2021. Transient variations in en route southern Indian ocean aerosols, Antarctic ozone climate and its relationship with HOx and NOx. Climate variability of southern high latitude regions. CRC Press: Boca Raton.

[63] Sonabawne, S.M., Devara, P.C.S., Meena, G.S., et al., 2021. Multiyear Measurements of Black Carbon Aerosols and Solar Radiation over Himadri, Ny-Alesund: Effects on Arctic Climate [Internet]. Understanding Arctic Environment: An Integrated Approach From Climate Change Perspective. Available from: http://www.essp.org/joint-projects/food/

[64] Crutzen, P.J., 2006. The anthropocene, earth system science in the anthropocene. Global Environmental Change and Food Systems GECAFS: A new interdisciplinary research project. Springer: Berlin,

Heidelberg. pp. 13-18.
[65] Overland, J.E., Wang, M., 2010. Large-scale atmospheric circulation changes are associated with the recent loss of Arctic sea ice. Tellus Ser A Dynamic Meteorology and Oceanography. 62, 1-9. DOI: https://doi.org/10.1111/j.1600-0870.2009.00421.x
[66] Francis, J.A., Vavrus, S.J., 2012. Evidence linking Arctic amplification to extreme weather in mid-latitudes. Geophysical Research Letters. 39(6). DOI: https://doi.org/10.1029/2012GL051000
[67] Denton, M.H., 2018. Northern hemisphere stratospheric ozone depletion caused by solar proton events: The role of the polar vortex. Geophysical Research Letters. 45, 2115-2124. DOI: https://doi.org/10.1002/2017GL075966
[68] Zuev, V.V., Savelieva, E., 2019. The role of the polar vortex strength during winter in Arctic ozone depletion from late winter to spring. Polar Science. 22,100469. DOI: https://doi.org/10.1016/j.polar.2019.06.001
[69] Pommereau, J.P., 2018. Recent Arctic ozone depletion: Is there an impact of climate change? Comptes Rendus Geoscience. 350, 347-353. DOI: https://doi.org/10.1016/j.crte.2018.07.009
[70] Damiani, A., 2020. Connection between antarctic ozone and climate: Interannual precipitation changes in the southern hemisphere. Atmosphere (Basel). 11(6), 579. DOI: https://doi.org/10.3390/atmos11060579
[71] Fogt, R.L., Marshall, G.J., 2020. The southern annular mode: Variability, trends, and climate impacts across the Southern Hemisphere. Wiley Interdisciplinary Reviews: Climate Change. 11(4), e652. DOI: https://doi.org/10.1002/wcc.652
[72] Krasouski, A., Zenchanka, S., 2018. Ozone layer depletion, climate change, risks and adaptation. Theory and practice of climate adaptation. Springer: Cham. pp. 137-150.
[73] Seckmeyer, G., Smolskaia, I., Pissulla, D., et al., 2009. Solar UV: Measurements and Trends. Twenty years of ozone decline. Springer: Dordrecht. pp. 359-368.
[74] Abas, N., 2018. Natural and synthetic refrigerants, global warming: A review. Renewable and Sustainable Energy Reviews. 90, 557-569. DOI: https://doi.org/10.1016/j.rser.2018.03.099
[75] Geller Marvin, A., Chanin, M.L., 2009. SPARC science supporting the montreal protocol. Twenty years of ozone decline. Springer: Dordrecht. pp. 393-403. DOI: https://doi.org/10.1007/978-90-481-2469-5_30
[76] Bais, A.F., 2018. Environmental effects of ozone depletion, UV radiation and interactions with climate change: UNEP environmental effects assessment panel. Photochemical and Photobiological Sciences. 17, 127-179. DOI: https://doi.org/10.1039/C7PP90043K
[77] Bernhard, G.H., 2020. Environmental effects of stratospheric ozone depletion, UV radiation and interactions with climate change: UNEP environmental effects assessment panel, update 2019. Photochemical and Photobiological Sciences. 19, 542-584. DOI: https://doi.org/10.1039/D0PP90011G
[78] Son, S.W., 2018. Tropospheric jet response to Antarctic ozone depletion: An update with Chemistry-Climate Model Initiative (CCMI) models. Environmental Research Letters. 13, 054024. DOI: https://doi.org/10.1088/1748-9326/aabf21
[79] Xie, F., 2018. An advanced impact of Arctic stratospheric ozone changes on spring precipitation in China. Climate Dynamics. 51, 4029-4041. DOI: https://doi.org/10.1007/s00382-018-4402-1
[80] Wuebbles Donald, J., 2009. Metrics for ozone and climate: Three-dimensional modeling studies of ozone depletion potentials and indirect global warming potentials. Twenty years of ozone decline. Springer: Dordrecht. pp. 297-326. DOI: https://doi.org/10.1007/978-90-481-2469-5_23
[81] Olsen, C.M., 2015. Cancers in Australia attributable to exposure to solar ultraviolet radiation and prevented by regular sunscreen use. Australian and New Zealand Journal of Public Health. 39, 471-476. DOI: https://doi.org/10.1111/1753-6405.12470
[82] Bais, A.F., 2015. Ozone depletion and climate change: Impacts on UV radiation. Photochemical and Photobiological Sciences. 14, 19-52. DOI: https://doi.org/10.1039/c4pp90032d
[83] Hayes, F., Sharps, K., Harmens, H., et al., 2020. Tropospheric ozone pollution reduces the yield of African crops. Journal of Agronomy and Crop Science. 206, 214-228. DOI: https://doi.org/10.1111/jac.12376
[84] Isaksen Ivar, S.A., Rognerud, B., 2009. Stratospheric ozone depletion and tropospheric chemistry. Twenty years of ozone decline. Springer: Dordrecht. pp. 279-290. DOI: https://doi.org/10.1007/978-90-481-2469-5_21
[85] Diffey, B.A., 2007. A contemporary strategy for sun exposure. Expert Review of Dermatology. 2, 139-142. DOI: https://doi.org/10.1586/17469872.2.2.139
[86] Anwar, F., A contemporary haudhry, F.N., Nazeer, S., et al., 2016. Causes of ozone layer depletion and its effects on human: Review. Atmospheric and Climate Sciences. 6, 129-134.

DOI: http://dx.doi.org/10.4236/acs.2016.61011

[87] UNEP Environmental Effects Panel, 1994. United Nations Environment Programme. Environmental Effects of Ozone Depletion: 1994 Assessment: Pursuant to Article 6 of the Montreal Protocol on Substances that Deplete the Ozone Layer [Internet]. Available from: https://wedocs.unep.org/20.500.11822/29033

[88] Norval, M., 2011. The human health effects of ozone depletion and interactions with climate change. Photochemical and Photobiological Sciences. 10, 199-225.
DOI: https://doi.org/10.1039/c0pp90044c

[89] Pearce, M.S., 2003. Skin cancer in children and young adults: 28 years' experience from the Northern Region Young Person's Malignant Disease Registry, UK. Melanoma Research. 13, 421-426.

[90] Wargent, J.J., Jordan, B.R., 2013. From ozone depletion to agriculture: Understanding the role of UV radiation in sustainable crop production. New Phytologist. 197, 1058-1076.
DOI: https://doi.org/10.1111/nph.12132

[91] Reddy, T.S., 2011. Ozone layer depletion and its effects: A review. International Journal of Environmental Science and Development. 2(1), 30-37.
DOI: http://dx.doi.org/10.7763/IJESD.2011.V2.93

[92] Li, F., Newman, P., Pawson, S., et al., 2018. Effects of greenhouse gas increase and stratospheric ozone depletion on stratospheric mean age of air in 1960-2010. Journal of Geophysical Research Atmospheres. 123, 2098-2110.
DOI: https://doi.org/10.1002/2017JD027562

[93] Godin Beekmann, S., 2009. International multi-instruments ground-based networks: Recent developments within the network for the detection of atmospheric composition changes. Twenty years of ozone decline. Springer: Dordrecht. pp. 135-156.
DOI: https://doi.org/10.1007/978-90-481-2469-5_10

[94] Yoshida, O., 2019. The international legal régime for the protection of the stratospheric ozone layer, second revised edition. Kluwer Law International: Netherlands.

[95] Albrecht, F., Parker, C.F., 2019. Healing the Ozone Layer: The montreal protocol and the lessons and limits of a global governance success story. Hart, p., Compton, M. (editors), Great policy successes. Oxford Academic: Oxford. pp. 304-322.
DOI: https://doi.org/10.1093/oso/9780198843719.003.0016

[96] Rowland, F.S., 2006. Stratospheric ozone depletion. Philosophical Transactions of the Royal Society B: Biological Sciences. 361, 769-790.
DOI: https://doi.org/10.1098/rstb.2005.1783

[97] Strahan, S.E., Douglass, A.R., 2018. Decline in antarctic ozone depletion and lower stratospheric chlorine determined from aura microwave limb sounder observations. Geophysical Research Letters. 45, 382-390.
DOI: https://doi.org/10.1002/2017GL074830

[98] Ravishankara, A., 2009. Findings from the 2006 ozone scientific assessment for the montreal protocol. Twenty years of ozone decline. Springer: Dordrecht. pp. 387-391.
DOI: https://doi.org/10.1007/978-90-481-2469-5_29

[99] Fow, A.J., 2006. Ozone Depletion and Global Warming [Master's thesis]. Hamilton: University of Waikato.

[100] Polvani, L.M., Previdi, M., England, M.R., et al., 2020. Substantial twentieth-century Arctic warming caused by ozone-depleting substances. Nature Climate Change. 10, 130-133.
DOI: https://doi.org/10.1038/s41558-019-0677-4

[101] Montzka, S.A., Reimann, S., Engel, A., et al., 2011. Ozone-depleting substances (ODSs) and related chemicals. Scientific Assessment of Ozone Depletion. 52, 1-112.

[102] Fang, X., 2019. Challenges for the recovery of the ozone layer. Nature Geoscience. 12, 592-596.
DOI: https://doi.org/10.1038/s41561-019-0422-7

[103] Bolaji, B.O., Huan, Z., 2013. Ozone depletion and global warming: Case for the use of natural refrigerant - A review. Renewable and Sustainable Energy Reviews. 18, 49-54.
DOI: https://doi.org/10.1016/j.rser.2012.10.008

[104] Fu, Q., Solomon, S., Pahlavan, H.A., et al., 2019. Observed changes in Brewer-Dobson circulation for 1980-2018. Environmental Research Letters. 14, 114026.
DOI: https://doi.org/10.1088/1748-9326/ab4de7

NASS
NAN YANG ACADEMY OF SCIENCES

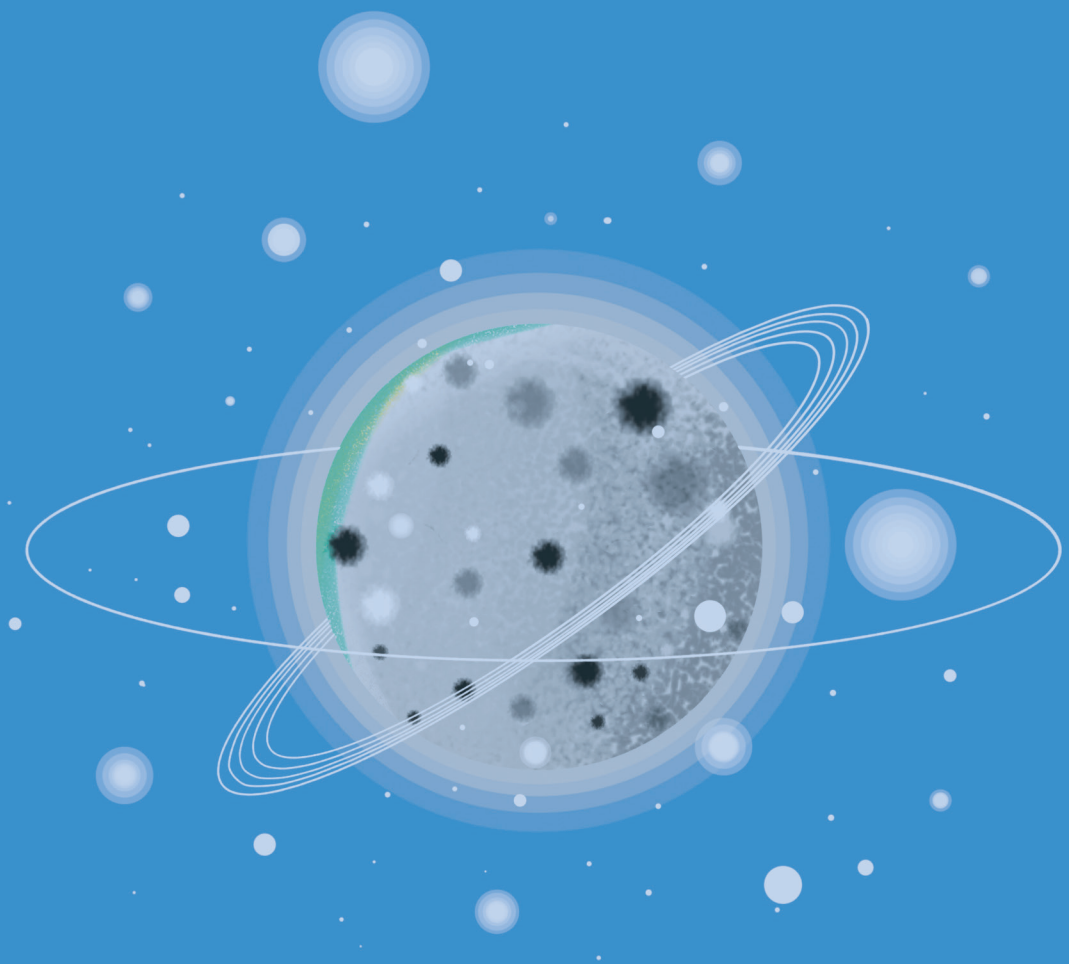

2810-9732
02
9 772810 973225

Tel.: +65 65881289
E-mail: eps@nassg.org
Website: ojs.nassg.org
Add.: 12 Eu Tong Sen Street #07-169 Singapore 059819